iScience

CellPress
OPEN ACCESS

Article

Adult-Onset Myopathy with Constitutive Activation of Akt following the Loss of hnRNP-U

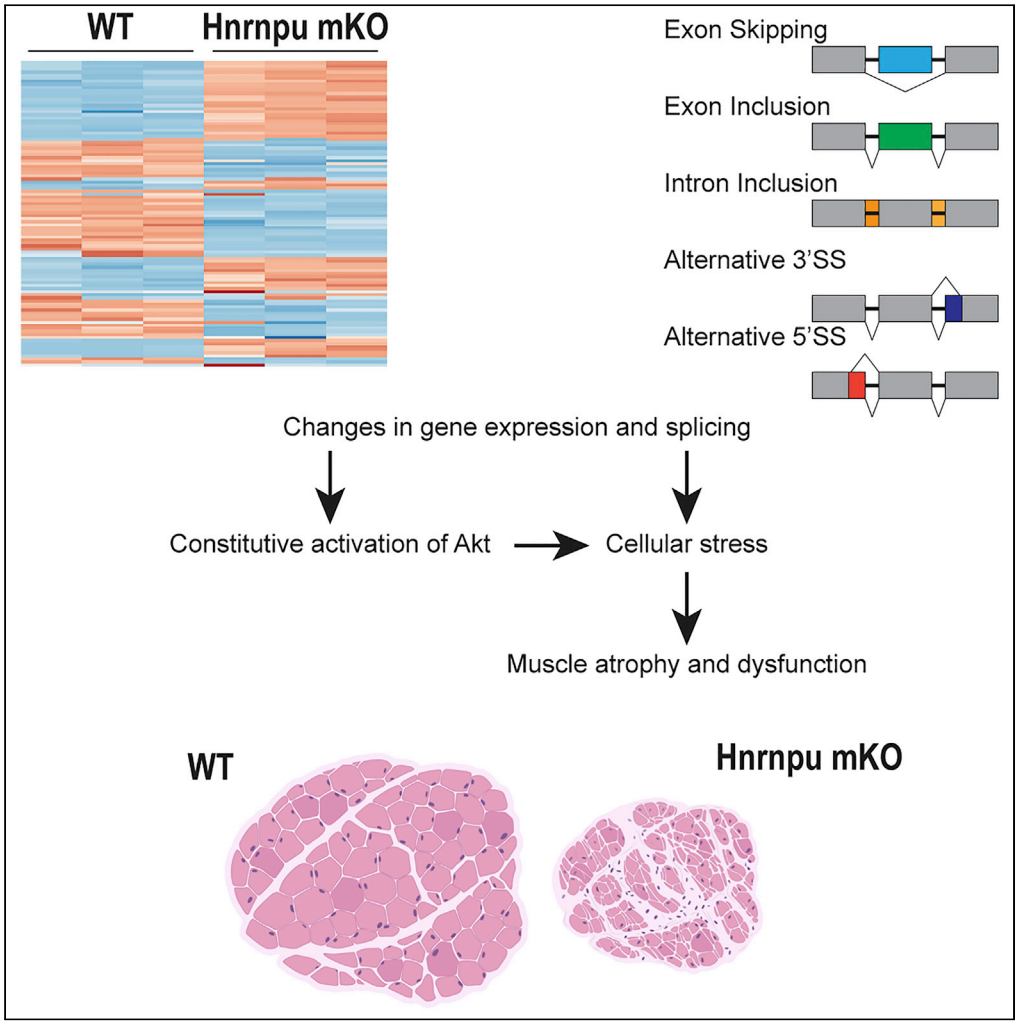

Debalina Bagchi, Benjamin D. Mason, Kodilichi Baldino, ..., Sherif El Raheb, Indranil Sinha, Ronald L. Neppl

rneppl@bwh.harvard.edu

HIGHLIGHTS

Hnrnpu mKO mice develop adult-onset myopathy with selective glycolytic muscle atrophy

Akt is constitutively active in the atrophied muscles of *Hnrnpu* mKO mice

Hnrnpu mutants show altered gene expression and alternative splicing patterns

Induction of genes associated with cellular and metabolic stress

Bagchi et al., iScience *23*, 101319
July 24, 2020
https://doi.org/10.1016/j.isci.2020.101319

iScience

CellPress
OPEN ACCESS

Article

Adult-Onset Myopathy with Constitutive Activation of Akt following the Loss of hnRNP-U

Debalina Bagchi,[1,4] Benjamin D. Mason,[3,4] Kodilichi Baldino,[2] Bin Li,[2] Eun-Joo Lee,[1] Yuteng Zhang,[2] Linh Khanh Chu,[3] Sherif El Raheb,[3] Indranil Sinha,[2] and Ronald L. Neppl[1,5,*]

SUMMARY

Skeletal muscle has the remarkable ability to modulate its mass in response to changes in nutritional input, functional utilization, systemic disease, and age. This is achieved by the coordination of transcriptional and post-transcriptional networks and the signaling cascades balancing anabolic and catabolic processes with energy and nutrient availability. The extent to which alternative splicing regulates these signaling networks is uncertain. Here we investigate the role of the RNA-binding protein hnRNP-U on the expression and splicing of genes and the signaling processes regulating skeletal muscle hypertrophic growth. Muscle-specific *Hnrnpu* knockout (mKO) mice develop an adult-onset myopathy characterized by the selective atrophy of glycolytic muscle, the constitutive activation of Akt, increases in cellular and metabolic stress gene expression, and changes in the expression and splicing of metabolic and signal transduction genes. These findings link *Hnrnpu* with the balance between anabolic signaling, cellular and metabolic stress, and physiological growth.

INTRODUCTION

Skeletal muscle has the remarkable ability to modulate its mass in response to the physiological changes associated with functional use, nutrient availability, systemic disease, and age. Under normal physiological conditions, skeletal muscle maintains its mass through a complex balance of anabolic and catabolic signaling (Glass, 2005). However, cachexia, metabolic dysfunction, muscular dystrophy, and advanced age lead to a disequilibrium between anabolic and catabolic signaling resulting in muscle dysfunction and atrophy (Cohen et al., 2015; Emery, 2002; Ernste and Reed, 2013; Marcell, 2003; Petruzzelli and Wagner, 2016). IGF-1/PI3K/Akt signaling has emerged as a key regulator of skeletal muscle hypertrophic growth and metabolism through its activation of mTOR-dependent anabolic processes while simultaneously inhibiting Foxo1/3-dependent catabolic processes (Manning and Toker, 2017). Transgenic overexpression of Akt1 in skeletal muscle promotes muscle hypertrophy (Lai et al., 2004), and its selective expression in glycolytic muscles promotes insulin sensitivity in aged mice that display impaired Akt activation (Akasaki et al., 2014). mTOR signals through two complexes, the mTOR containing complex 1 (mTORC1), which both activates anabolic processes while inhibiting autophagy, and the mTOR containing complex 2 (mTORC2), which is the primary Akt1 Ser473 kinase (Manning and Toker, 2017). Although the molecular regulation is complex, changes in Akt and mTOR signaling contribute to metabolic derangements and muscle wasting (Castets et al., 2013; Risson et al., 2009; Saxton and Sabatini, 2017).

Alternative splicing is a key gene regulatory mechanism whereby the differential inclusion of exons results in multiple mRNA isoforms from a single genomic locus. This process plays a crucial role in the post-transcriptional regulation of gene and protein isoform expression (Lee and Rio, 2015) and is differentially regulated in response to cellular stress (Biamonti and Caceres, 2009; Dutertre et al., 2011). Current analyses indicate that >95% of human multi-exon genes are subject to alternative splicing (Pan et al., 2008). Brain, heart, and skeletal muscle have the highest levels of evolutionary conserved alternatively spliced transcripts (Merkin et al., 2012) and are subject to multiple disorders due to mis-splicing events (Faustino and Cooper, 2003; Scotti and Swanson, 2016). Alternative splicing in skeletal muscle plays a crucial role in muscle development, and genetic mutations in both splice sites and the RNA binding proteins that modulate splicing play causal roles in the pathogenesis of neuromuscular disorders (Ho et al., 2005; Lin et al., 2006; Philips

[1]Department of Orthopaedic Surgery, Brigham and Women's Hospital, Harvard Medical School, 75 Francis Street, Boston, MA 02115, USA

[2]Division of Plastic Surgery, Department of Surgery, Brigham and Women's Hospital, Harvard Medical School, 75 Francis Street, Boston, MA 02115, USA

[3]Department of Orthopaedic Surgery, Brigham and Women's Hospital, 75 Francis Street, Boston, MA 02115, USA

[4]These authors contributed equally

[5]Lead Contact

*Correspondence: rneppl@bwh.harvard.edu

https://doi.org/10.1016/j.isci.2020.101319

et al., 1998; Runfola et al., 2015). In addition, dysregulated splicing is increasingly recognized as a causal factor promoting cellular dysfunction through changes in the binding properties, enzymatic activities, and intracellular localization of a large percentage of the proteome (Tress et al., 2007). However, our understanding of how alternative splicing modulates the activity of IGF-1/PI3K/Akt signaling in skeletal muscle physiology is limited.

The functionally diverse heteronuclear ribonucleoprotein (hnRNP) family of RNA-binding proteins play key roles in RNA metabolism including mRNA stabilization and the regulation of alternative splicing (Geuens et al., 2016; Martinez-Contreras et al., 2007). Genetic mutations and dysregulated expression of hnRNPs A1, E1/2 (PCBP1/2), I (PTBP1), P2 (FUS), and Q (SYNCRIP) are implicated in the molecular pathogenesis of neuromuscular disorders including myotonic and limb girdle muscular dystrophy, amyotrophic lateral sclerosis, and spinal muscle atrophy (Geuens et al., 2016; Li et al., 2020; Vance et al., 2009). HnRNP family member U (hnRNP-U) is the largest member of the hnRNP family, ubiquitously expressed, and known to modulate both mRNA stability and alternative splicing (Huelga et al., 2012; Xiao et al., 2012; Yugami et al., 2007). Clinically, heterozygous loss-of-function mutations in the *Hnrnpu* gene are associated with craniofacial anomalies, developmental delays, and seizures (Yates et al., 2017). In mice, genetic deletion of *Hnrnpu* specifically within cardiomyocytes leads to a dilated cardiomyopathy phenotype around postnatal day 14 (Ye et al., 2015). Here, we identify hnRNP-U as being essential for skeletal muscle hypertrophic growth, in part, through modulating the balance between Akt1-dependent anabolic signaling and the energy and nutrient availability to support hypertrophic growth. hnRNP-U expression is repressed with age and necessary for the proper expression and splicing of genes critical for metabolic and growth processes.

RESULTS

The Development and Early Postnatal Growth of Skeletal Muscle Is Phenotypically Normal in the Absence of Hnrnpu

The hnRNP-U protein is expressed in nearly all tissues examined in the adult mouse (Figure 1A). However, the expression of hnRNP-U in skeletal muscle decreases abruptly in aged mice (Figure 1B). To study the role of hnRNP-U in skeletal muscle growth and function, we crossed Hnrnpu$^{fl/fl}$ mice (Ye et al., 2015) with a mouse line expressing the Cre recombinase under the control of the human skeletal actin promoter (HSA-Cre). HSA-Cre expression starts at E8.5 and continues into adulthood (Miniou et al., 1999). Consistent with a prior report in which *Hnrnpu* was deleted in both cardiac and skeletal muscle during development (Ye et al., 2015), Hnrnpu$^{fl/fl}$;HSA-Cre (mKO) mice are born in normal Mendelian ratios with no observable abnormalities (Figure S1). However, in contrast with this prior report, *Hnrnpu* mKO mice continue to develop normally past postnatal day 14 (P14). Western blot analysis indicates ~50% reduction in hnRNP-U expression in Hnrnpu mutants at P21 (Figure 1C). Laminin stained sections of P21 *Hnrnpu* mutant gastrocnemius (GSN, Figure 1D) and soleus (Figure 1G) are morphologically indistinguishable from littermate controls. Although subtle differences are observed in the myofiber size distribution curves of the gastrocnemius (Figure 1E) and soleus (Figure 1H), there are no statistically significant differences in the average myofiber cross-sectional areas (Figures 1F and 1I). Furthermore, we observe no differences in the morphology, myofiber size distribution, or the average myofiber cross-sectional area of the tibialis anterior (TA) of Hnrnpu mKO mice at P21 (Figure S2). Collectively, these data indicate embryonic deletion of *Hnrnpu* does not measurably impact the development or post-natal growth of skeletal muscle up to ~P21.

Hnrnpu mKO Mice Develop a Severe Adult-Onset Myopathy

To explore the role of *Hnrnpu* on skeletal muscle and whole-body growth, we performed longitudinal body weight analyses starting at P21. Consistent with our analyses of mice at P21 (Figure 1), male and female mKO mice are indistinguishable by weight from littermate controls up to approximately 4 weeks of age (Figure 2A). Growth curve analyses indicate that *Hnrnpu* mKO mice reach a body weight plateau at approximately 11–13 weeks of age, with statistically significant reductions in the body weights of males and females by 6- and 12-weeks of age, respectively. Male and female *Hnrnpu* mutants become visually distinguishable from control littermates by 10–12 weeks and 16–18 weeks, respectively. Functional assessments at 3 months of age indicate that *Hnrnpu* mutants have significant reductions in grip strength (Figure 2B) and maximal running speed (Figure 2C). Consistent with these analyses, the normalized muscle mass of *Hnrnpu* mutants is observed to be significantly reduced with respect to littermate controls (Figure 2D).

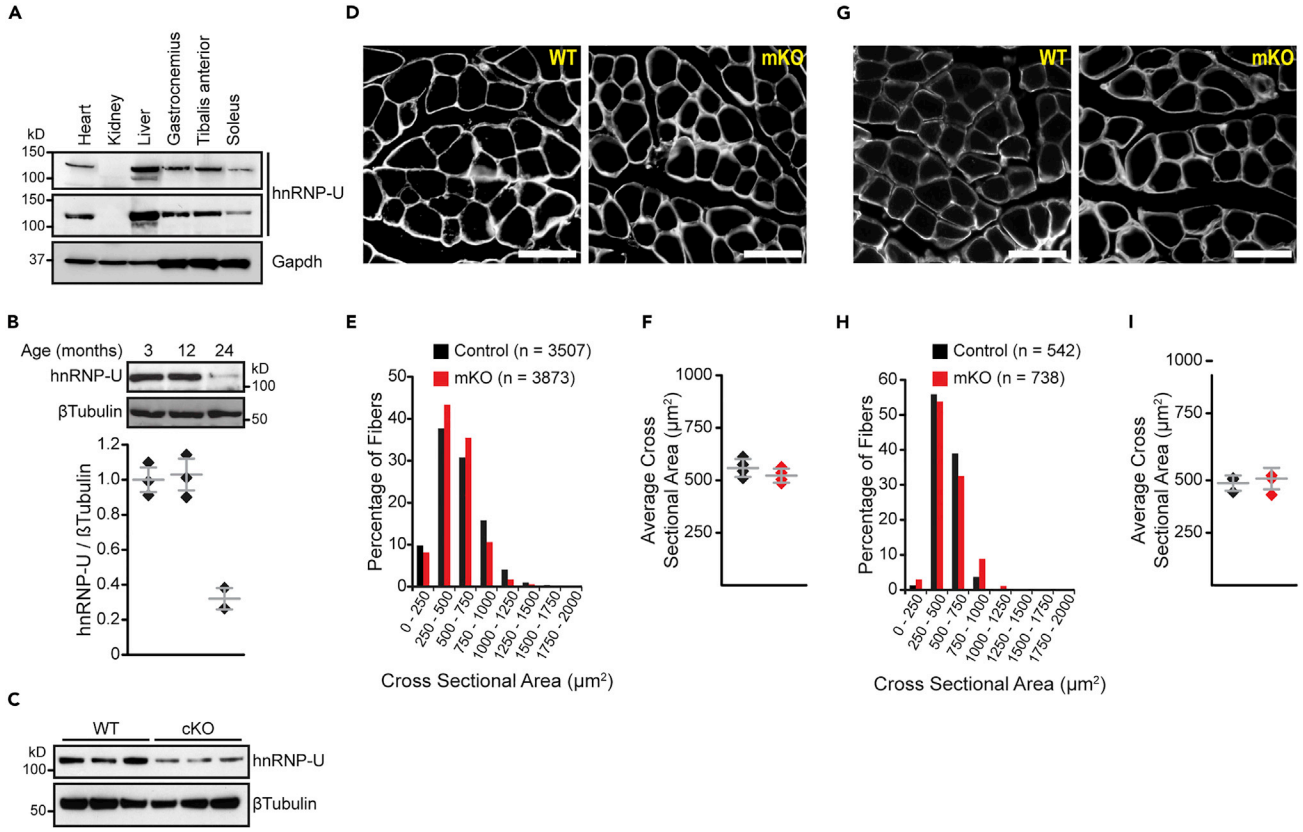

Figure 1. *Hnrnpu* mKO Mice Are Born Phenotypically Normal

(A) Representative western blots of relative hnRNP-U expression in adult mouse tissues. Data are from n = 2 biological replicates.

(B) Representative western blot and quantification of hnRNP-U expression in the gastrocnemius with advancing age. Data are from n = 3 WT male mice at 3 and 12 months of age, and n = 2 WT male mice at 24 months of age.

(C) Western blot of hnRNP-U expression in gastrocnemius muscle at P21.

(D–I) Data are from n = 3 control and n = 3 mKO male mice at P21. (D–F) Immunohistological analyses of gastrocnemius muscle. (G–I) Immunohistological analyses of soleus muscle. (D and G) Laminin staining of muscle transverse sections. The scale bar is 50 μm. (E and H) Myofiber size distribution curves. (F and I) Average myofiber cross-sectional areas. Data are mean ± standard deviation. Significance (*) was set at $p < 0.05$. p Values were calculated using the Student's two-tailed t test assuming unequal variances.

Histological examination of muscles from *Hnrnpu* mutants at 3 months of age reveals central nuclei, myofiber degeneration and necrosis, intracellular inclusions, and extensive fibrosis (Figures 2E–2I). H&E staining of *Hnrnpu* mutant gastrocnemius muscles reveals the accumulation of mononuclear cells and intracellular inclusions (Figure 2E). In the TA we observe myofiber degeneration, intracellular inclusions, and abundant central nuclei (Figure 2F). Quantification of H&E images indicate that 6.45 ± 1.88% of TA myofibers in *Hunrnpu* mutants contain central nuclei as compared with 0.19 ± 0.24% of control myofibers (Figure 2G). Masson's Trichrome staining of both the TA and gastrocnemius muscles indicate that *Hnrnpu* mutants have extensive fibrosis (Figure 2H). Quantification of Masson's staining indicate that the fibrotic area of TA and gastrocnemius muscles increase from 4.0 ± 0.67% and 3.4 ± 0.89% in controls to 11.8 ± 2.13% and 20.3 ± 4.78% in *Hnrnpu* mutants (Figure 2I), respectively. As *Hnrnpu* mutants age, female mice present with pronounced kyphosis by 5 months, whereas males develop a less severe form by 7 months (Figure S3).

To further characterize the muscle architecture of Hnrnpu mutants, we next performed quantitative analyses of myofiber cross-sectional areas. Immunofluorescence labeling of laminin and quantification of gastrocnemius myofiber cross-sectional areas indicate myofiber atrophy in mutant mice, as indicated by an elevated leftward shift of the myofiber size distribution curve (Figures 3A and 3B). Quantitatively, data indicate a significant 21.2% decrease (1479 ± 29 versus 1878 ± 150 μm^2, $p = 0.011$, mKO versus control) in the average gastrocnemius myofiber cross-sectional area of individual mice (Figure 3C). In contrast, the tibialis anterior has only a subtle leftward shift of the myofiber size distribution curve (Figures 3D and

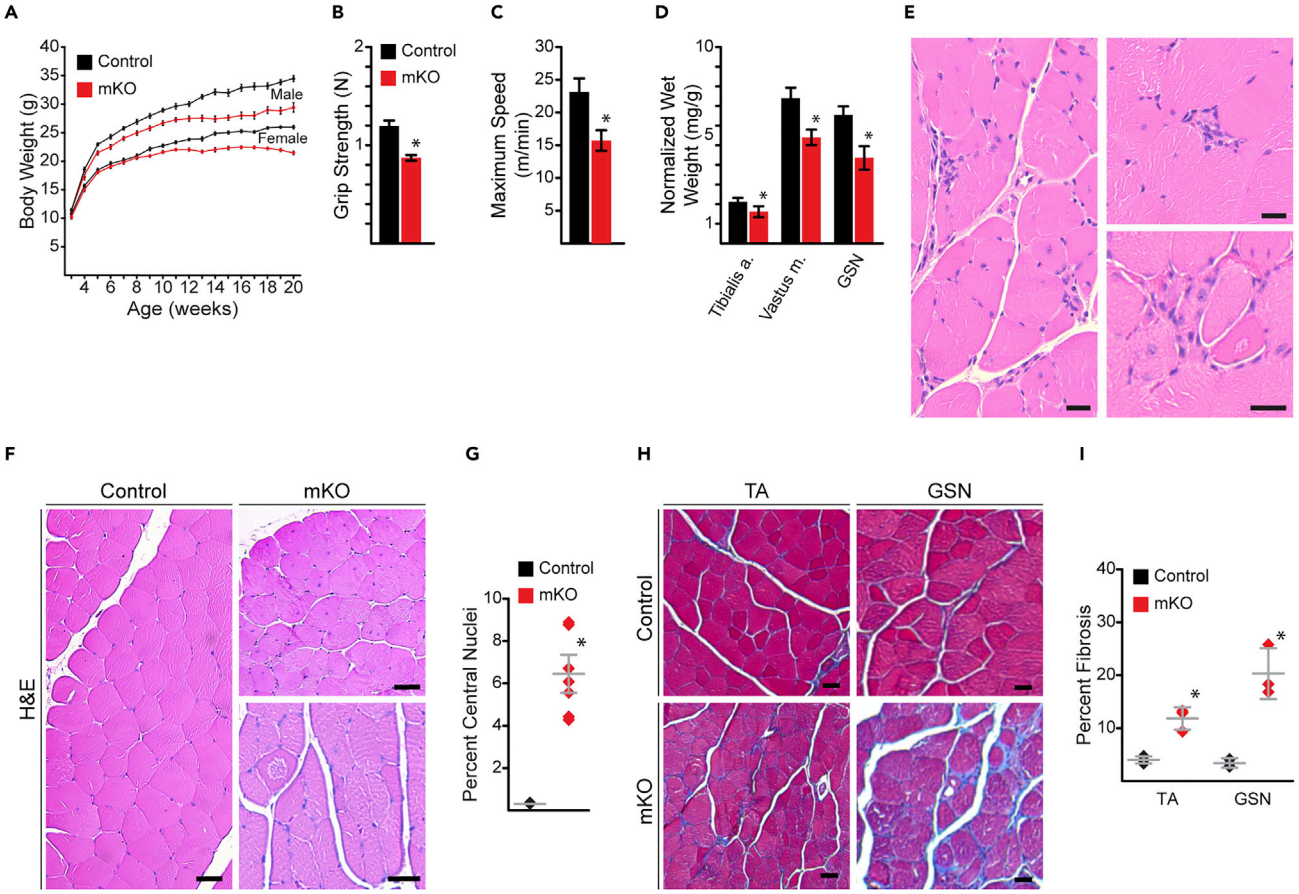

Figure 2. *Hnrnpu* mKO Mice Develop Adult-Onset Myopathy

(A) Growth curves of male and female mice. Data are mean ± SEM from 25–40 mice per genotype, depending on age and gender.

(B) Grip strength.

(C) Maximum running speed.

(D) Normalized muscle wet weight.

(B–D) Data are mean ± standard deviation from n = 8 control and n = 8 mKO male mice. Significance (*) was set a $p < 0.05$.

(E–I) Histological analyses of *Hnrnpu* mutant and control littermates at 3 months of age.

(E) H&E staining of *Hnrnpu* mutant gastrocnemius muscle. The scale bar is 50 μm.

(F) H&E staining of tibialis anterior. The scale bar is 50 μm.

(G) Quantification of central nuclei in tibialis anterior. Data are from n = 9,785 control and n = 9,921 mutant myofibers from n = 7 male mice per group. Data are mean ± standard deviation. Significance (*) was set at $p < 0.05$.

(H) Masson's Trichrome staining of tibialis anterior and gastrocnemius. The scale bar is 50 μm.

(I) Quantification of percent fibrotic area. Data are mean ± standard deviation from n = 3 control and n = 3 male mKO mice. Significance (*) was set at $p < 0.05$. p Values were calculated using the Student's two-tailed t test assuming unequal variances.

3E), whereas the soleus is virtually indistinguishable (Figures 3G and 3H) between mKO and littermate controls. Although we observe decreases of 7.9% (1,541 ± 76 versus 1,674 ± 114 μm^2, p = 0.058, mKO versus control) and 3.3% (725 ± 94 versus 701 ± 98 μm^2, p = 0.537, mKO versus control) in the tibialis anterior (Figure 3F) and soleus (Figure 3I), respectively, these differences fail to reach statistical significance. Consistent with these observations, NMR body composition analyses indicate a significant decrease in the lean muscle mass of *Hnrnpu* mutants as compared with littermate controls (Table 1). Collectively, these observations indicate that the loss of *Hnrnpu* results in a multifaceted myopathy characterized by histological features of myofiber necrosis and inclusions, central nuclei, extensive fibrosis, and muscle wasting.

Hnrnpu Mutant Mice Have an Impaired Regenerative Response

The decreased lean muscle mass and leftward shift of myofiber size distribution, in conjunction with an increase in myofibers with centrally located nuclei, prompted us to evaluate the capacity for myofiber

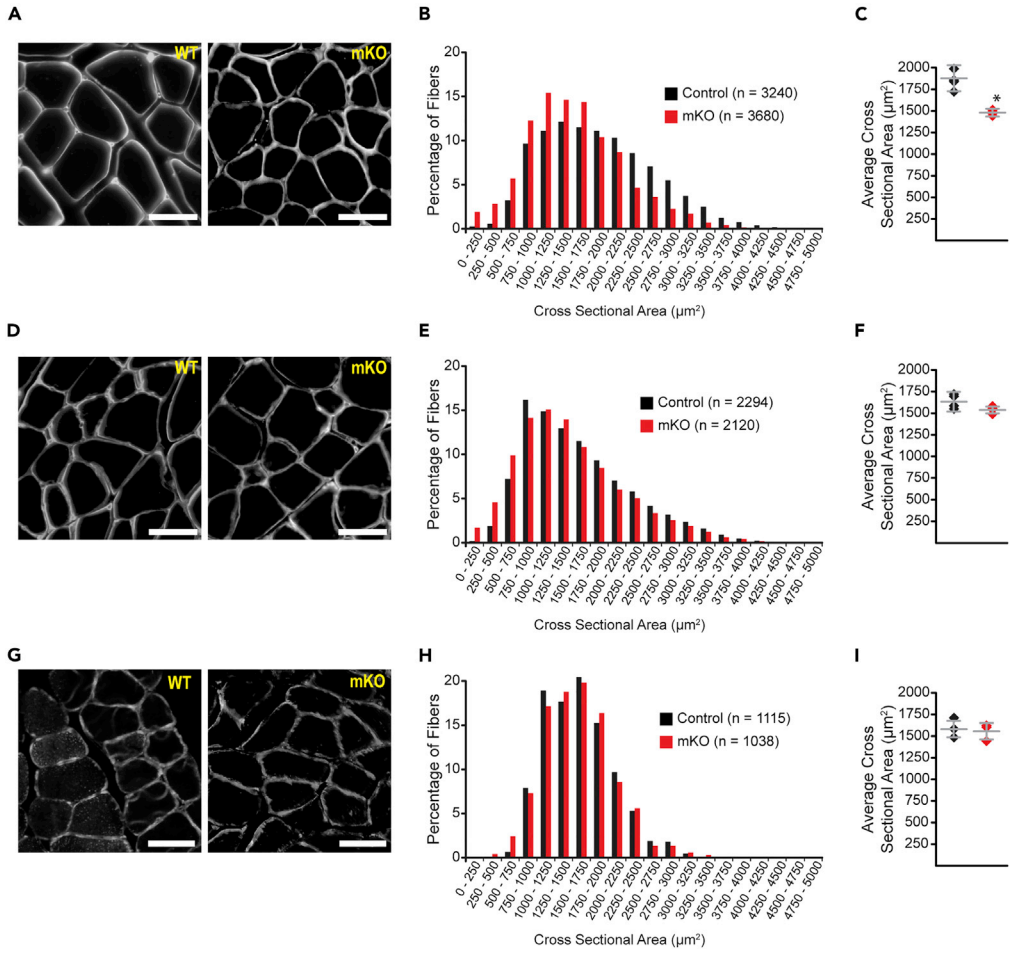

Figure 3. Selective Muscle Wasting in *Hnrnpu* Mutants

(A–C) Immunohistological analyses of gastrocnemius muscle.

(D–F) Immunohistological analyses of tibialis anterior muscle.

(F–I) Immunohistological analyses of soleus muscle.

(A, D, and G) Laminin staining of muscle transverse sections. The scale bar is 50 μm.

(B, E, and H) Myofiber size distribution curves.

(C, F, and I) Average myofiber cross-sectional areas.

(A–I) Data are from n = 4 control and n = 4 mKO male mice at 3 months of age. Data are mean ± standard deviation. Significance (*) was set at $p < 0.05$. p Values were calculated using the Student's two-tailed t test assuming unequal variances.

regeneration following injury in *Hnrnpu* mutant mice. Morphometric analysis of wild-type (WT) control mice 10 days post injury (DPI) depicts robust regeneration characterized by large well-organized myofibers. In contrast, mKO mice exhibit an impaired regenerative response as indicated by numerous small poorly organized myofibers (Figure 4A). Quantitative analyses of histological sections indicate a leftward shift in the myofiber size distribution curve of newly regenerated myofibers in mKO mice relative to controls (Figure 4B). To explore whether the age-associated loss of hnRNP-U (Figure 1B) contributes to the regenerative deficits of aged muscles (Demontis et al., 2013), we performed the cryoinjury model on young (3 months) and old (24–26 months) C57BL/6 WT mice. Morphometric analyses of H&E-stained sections obtained from young mice exhibit a robust regenerative response at 10 DPI as evidenced by large well-organized regenerated myofibers, whereas old mice exhibit a weak regenerative response characterized by small, poorly organized myofibers (Figure 4C). Quantitative analyses of histological sections indicate a leftward shift in the myofiber size distribution curve of newly regenerated myofibers in aged mice relative to young controls (Figure 4D). Overall, the newly regenerated myofibers of young mKO mice are 32% smaller (903 ± 261 versus 1,339 ± 174, mKO versus control) than littermate controls, whereas the

	WT (n = 7)	mKO (n = 7)	p Value
Body weight (g)	28.61 ± 1.46	25.70 ± 1.39	0.014
Fat (g)	3.45 ± 0.52	3.44 ± 0.57	0.995
Lean (g)	24.26 ± 1.50	21.33 ± 1.51	0.019
Free water (g)	0.17 ± 0.10	0.14 ± 0.08	0.604
Total water (g)	18.31 ± 1.03	14.94 ± 1.14	0.003

Table 1. NMR Body Composition Parameters of Hnrnpu mKO Mice at 3 Months of Age

Related to Figure 2. Data are mean ± standard deviation from n = 7 mice per group. p Values were calculated using the Student's two-tailed t test assuming unequal variances.

newly regenerated myofibers of old C57BL/6 WT mice are 35% smaller (833 ± 44 versus 1,298 ± 168 μm^2, old versus young) than young C57BL/6 controls (Figure 4E). Collectively, these observations indicate that *Hnrnpu* mutants have a regenerative response with many similarities to that of aged mice, suggesting that the loss of hnRNP-U in advanced age may contribute to regenerative impairments.

Loss of Hnrnpu Leads to Dysregulated Expression and Splicing of Metabolic Genes

To better understand the molecular processes underlying our observations, we performed whole transcriptome gene and splice variant expression analyses on the gastrocnemius muscles of mice at 3 months of age. We obtained >60 million strand-specific 150-bp paired-end reads per sample with at least 91% of reads mapping to the mouse genome. Differential gene expression (log2FoldChange ±1.0, padj <0.01) analysis indicate 1,171 and 786 genes are increased and decreased in expression (mKO versus control), respectively (Figure 5A). Quantitative PCR validation of RNA sequencing (RNA-seq) analyses (data not shown) indicate a marked reduction in the expression of Myostatin, as well as a general repression of the E3 ubiquitin ligases and accessory proteins known to promote muscle atrophy (Bodine et al., 2001; Nowak et al., 2019; Sartori et al., 2013). In addition, genes associated with increased energy expenditures and metabolic stress, including *Sln*, *Asns*, *Fgf21*, *Gdf15*, *Psat1*, and *Mthfd2* (Balasubramanian et al., 2013; Chung et al., 2017; Fisher and Maratos-Flier, 2016; Maurya et al., 2018; Nilsson et al., 2014), are robustly induced in the muscles of *Hnrnpu* mutants (Figure 5B). Interestingly, the induction of long non-coding RNAs (lncRNAs) appears to portend muscle atrophy and/or metabolic dysfunction, as we observe >3-fold more lncRNAs to be induced (Log2FoldChange >2, padj <0.01), rather than repressed. To better understand the cellular and molecular processes impacted by the changes in gene expression we performed Gene Ontology enrichment analysis. Our analysis indicates that up-regulated genes are highly associated with inflammatory signaling (Figure S4A), whereas downregulated genes are associated with energy production and metabolic processes (Figure S4B). Specifically, we note the marked repression of *Mss51* (Zmynd17), which acts as an inhibitor of oxidative metabolism (Rovira Gonzalez et al., 2019), multiple solute transporters with roles in amino acid and anion/cation (*Slc15a5, Slc30a2, Slc40a1, Slc4a10*) homeostasis (Lin et al., 2015), as well as multiple enzymes involved in the biogenesis of triacylglycerol (*Dgat2l6*) (Yen et al., 2008), amino acids (*Gadl1*, *Padi2*, *Amd1/2*), and glycogen (*Gys2*) (Figure 5C). The top induced and repressed genes in the gastrocnemius of mKO mice are listed in Table S1.

We next examined the impact of *Hnrnpu* deletion on alternative splicing from the strand-specific paired-end RNA-seq data. Using the rMATS program for splicing analysis (Shen et al., 2014), we identified 2,909 significant alternative splicing events (|ΔPSI| > 0.1, false discovery rate [FDR] < 0.01; Table S2). The distribution of these events, which include skipped exons (SEs), retained introns (RIs), mutually exclusive exons (MXEs), and the use of alternative 5′ (A5SS) and 3′ (A3SS) splice sites, is shown in Figure 5D. These data show that loss of hnRNP-U leads to extensive dysregulation of exon utilization in which SE (74.2%) and MXE (11.7%) events far exceed the utilization of alternative exons (A5SS and A3SS), suggesting that hnRNP-U may be involved in defining intron/exon boundaries. This is in contrast with a prior study in the developing heart, in which RI events were the largest share of alternative splicing events following the loss of hnRNP-U (Ye et al., 2015), thus suggesting that the role of hnRNP-U in pre-mRNA splicing modulation is differentially regulated in a cell type- and context-dependent manner. Coupled with the differential gene expression analysis, we observe 1,296 mis-splicing events (FDR < 0.01) across 710 genes whose expression is significantly altered (padj <0.01) in the absence of *Hnrnpu* (Figure 5E). The majority of

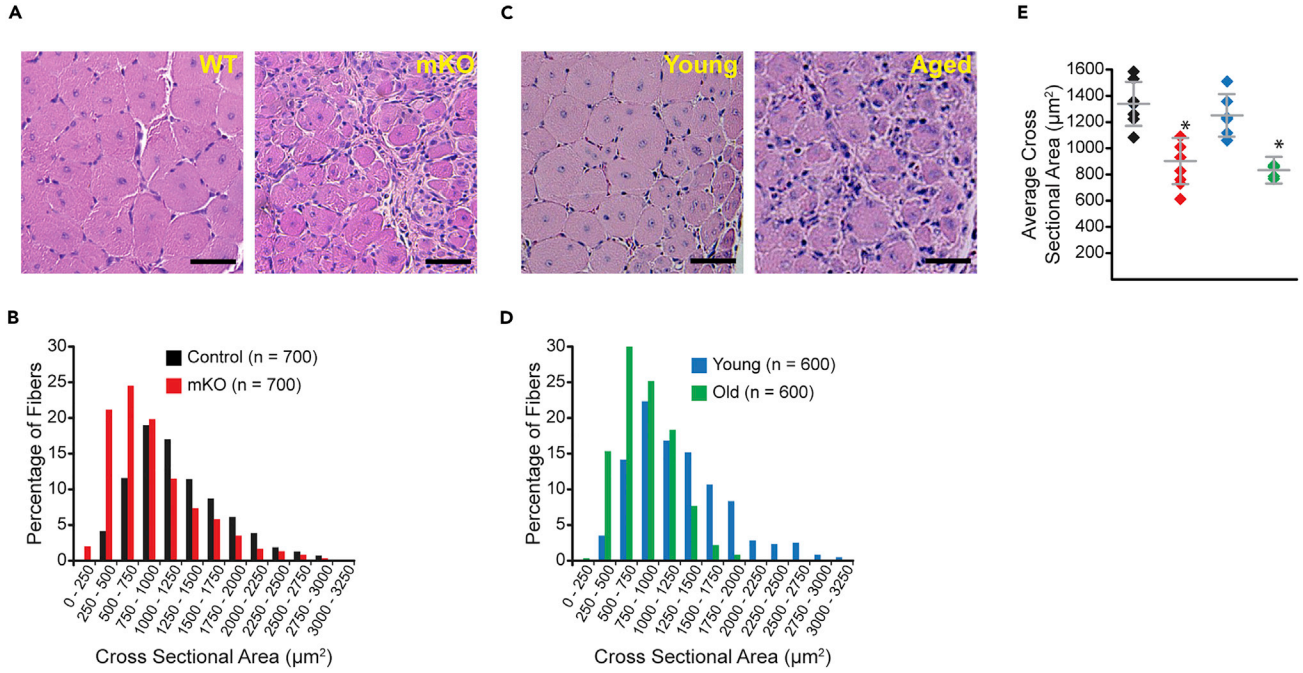

Figure 4. Young *Hnrnpu* mKO Mice Phenocopy the Regenerative Response of Old Mice

(A) H&E-stained transverse sections of young (3 months) control and mKO tibialis anterior muscle 10 days post injury. The scale bar is 50 μm.

(C) H&E-stained transverse sections of young (3 months) and old (26 months) tibialis anterior muscles 10 days post injury. The scale bar is 50 μm.

(B) Myofiber size distribution curve of regenerating myofibers from (A).

(D) Myofiber size distribution curve of regenerating myofibers from (C).

(E) Dot plot of average regenerated myofiber cross-sectional area from n = 7 young *Hnrnpu* control (black diamond), n = 7 young male *Hnrnpu* mKO (red diamond), n = 6 young C57BL/6 (blue diamond), and n = 6 old male C57BL/6 mice (green diamond). Bars are mean ± standard deviation. Significance (*) was set at $p < 0.05$. p Values were calculated using the Student's two-tailed t test assuming unequal variances.

these events occur on genes whose expression is decreased (985 events across 529 genes) as compared with those that are increased (311 events across 181 genes). Splicing events in mKO mice are biased toward exclusion (ΔPSI, quadrant I: 228 events across 150 genes, quadrant IV: 653 events across 388 genes) rather than inclusion (-ΔPSI, quadrant II: 83 events across 56 genes, quadrant III: 332 events across 218 genes). To better understand the cellular and molecular processes impacted by the changes in alternative splicing, we again performed Gene Ontology enrichment analysis. Our analysis indicates that genes with the differential inclusion/exclusion of exons ($|\Delta PSI| > 0.1$, FDR < 0.01) are highly associated with metabolic and signal transduction processes (Figure S4C). In addition, Gene Ontology enrichment analysis of genes that are both downregulated and mis-spliced (Figure 5E) similarly indicate that this subset of genes is highly associated with metabolic and signal transduction processes (Figure S4D).

A more detailed examination of altered splicing events revealed that hnRNP-U is necessary for normal exon utilization in multiple genes, including *Senp1* (Figure 5F), *Setd3* (Figure 5G), *Mff* (Figure 5H), *Sorbs1* (Figure 5I), and *Inpp4a* (Figure 5J). The Sentrin/SUMO-specific protease 1 (*Senp1*) has been previously shown to be involved in regulating mitochondrial biogenesis through enhancing PGC-1α activity (Cai et al., 2012), whereas mitochondrial fission factor (*Mff*) is a critical regulator of mitochondrial dynamics (Otera et al., 2010). Expression of SET domain containing methyltransferase 3 (*Setd3*) is positively correlated with skeletal muscle hypertrophy (Seaborne et al., 2018) and involved in muscle differentiation via promoting the expression of the myogenic regulatory factors MyoG and Myf6 (Eom et al., 2011). Sorbin and SH3 domain containing protein 1 (*Sorbs1*) is required for PI3K-independent, insulin-stimulated glucose uptake (Baumann et al., 2000), whereas the inositol polyphosphate-4-phosphatase 1A (*Inpp4a*) is a PIP2 phosphatase impairing Akt activation (Ivetac et al., 2009). Collectively, these data indicate that *Hnrnpu* is required for the expression and splicing of genes involved in the signal transduction and metabolic processes crucial for normal skeletal muscle growth.

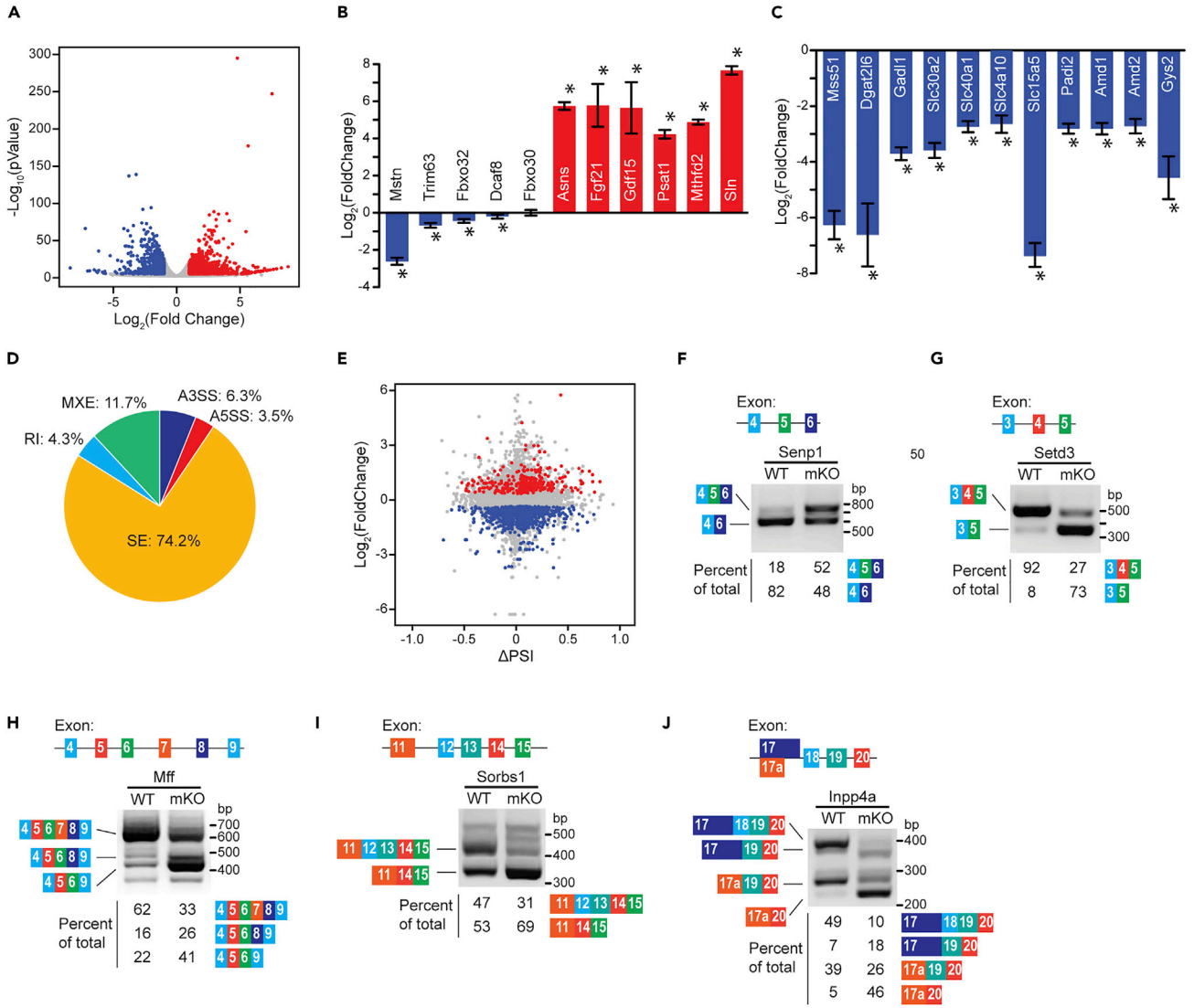

Figure 5. Gene Expression and Alternative Splicing Are Dysregulated in *Hnrnpu* mKO Mice

(A) Whole-genome expression profile of male *Hnrnpu* mutant gastrocnemius. Red and blue dots depict increased and decreased gene expression (mKO versus control, padj <0.01), respectively. Decreased (blue) and increased (red) expression of genes in *Hnrnpu* mutant gastrocnemius associated with (B) muscle atrophy and metabolic stress, and (C) energy production and nutrient transport.

(B and C) Data are Log_2(FoldChange) ± standard error. Significance (*) was set at $p < 0.0001$. p Values were calculated using the Wald test corrected for multiple testing using the Benjamini-Hochberg method.

(D) Summary of significant differential splicing events between genotypes. $|\Delta PSI| > 0.1$, FDR < 0.01.

(E) Whole-genome expression profiling of mis-spliced differentially expressed genes in (A). Dots represent individual splicing events occurring on differentially expressed genes. Statistically significant splicing events (FDR < 0.01) occurring on statistically significant differentially expressed genes (padj <0.01) are highlighted in red. p Values were calculated using a likelihood-ratio test.

(F–J) Examples of differential splicing regulated by hnRNP-U: *Senp1* (F), *Setd3* (G), *Mff* (H), *Sorbs1* (I), and *Inpp4a* (J). SE, Skipped Exon; RI, Retained Intron; MXE, Mutually Exclusive Exon; A3SS, Alternative 3′ Splice Site; A5SS, Alternative 5′ Splice Site.

Akt Signaling Is Constitutively Active in Hnrnpu Mutants

To further explore the impact of *Hnrnpu* deletion on the signal transduction and metabolic processes underlying the muscle wasting in *Hnrnpu* mutants, we examined IGF-1/PI3K/Akt signaling. To begin, we injected either saline or recombinant IGF-1 into the gastrocnemius muscles of control and mutant mice at ~4 months of age. Quantitative western blot analyses indicate that IGF-1 receptor (IGF-1R) autophosphorylation in response to IGF-1 administration is similar between *Hnrnpu* mutant and control mice (Figures 6A and 6B), suggesting that initiation of the IGF-1/PI3K/Akt1 signaling cascade is intact in the absence of

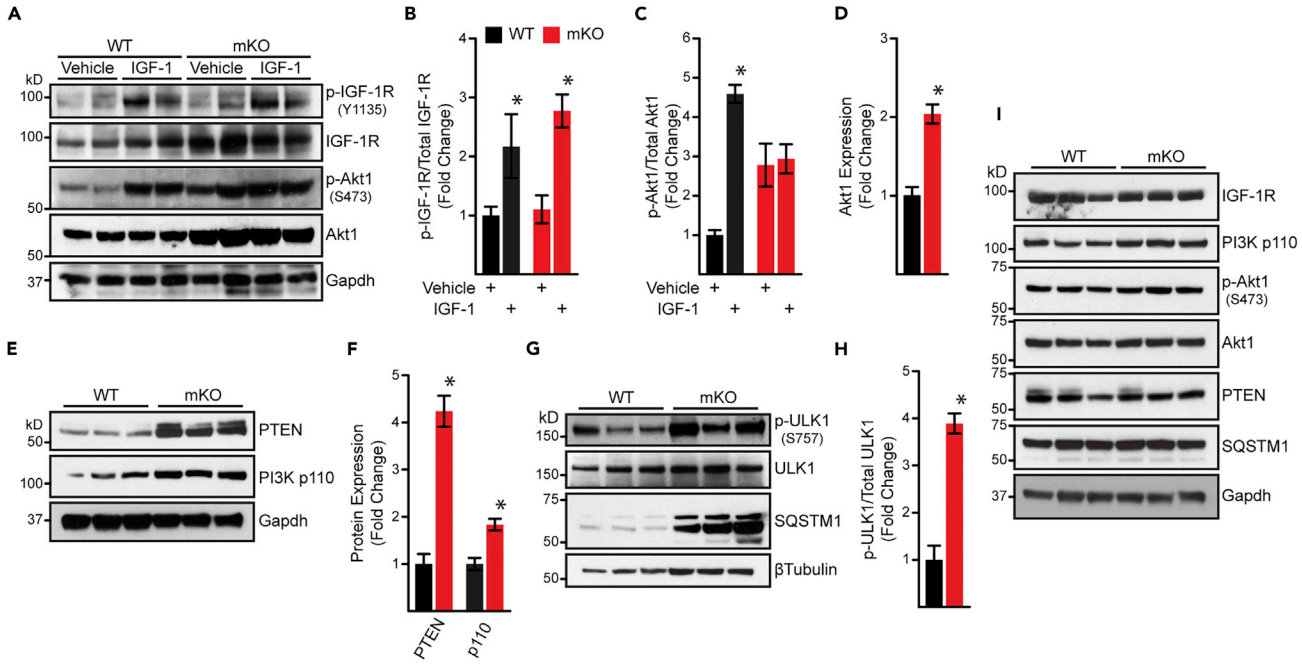

Figure 6. Constitutive Activation of Akt1 and Impaired Autophagic Flux in *Hnrnpu* mKO Mice

(A) Representative western blots of gastrocnemius muscle lysates 1 h following injection of IGF-1.

(B–D) Quantification of (A). Data are mean ± standard deviation from n = 3 independent experiments and are normalized to WT vehicle controls. Significance (*) was set at $p < 0.05$. p Values were calculated using the Student's two-tailed t test assuming unequal variances.

(E and G) Representative western blots of unstimulated gastrocnemius muscles at 3 months of age.

(F and H) Quantification of (E) and (G), respectively. Data are mean ± standard deviation from n = 3 biological samples per genotype and are normalized to WT controls. Significance (*) was set at $p < 0.05$. p Values were calculated using the Student's two-tailed t test assuming unequal variances.

(I) Representative western blots of unstimulated gastrocnemius muscles at P21. Male mice were used for all analyses.

Hnrnpu. Upon examination of Akt1 phospho-activation, we observe that IGF-1 stimulation induces a robust induction in Akt1 phosphorylation at Ser473 in control mice (Figures 6A and 6C), indicating that IGF-1 stimulation results in the phospho-activation of Akt1. In contrast, we observe that the level of Akt1 Ser473 phosphorylation in vehicle-treated *Hnrnpu* mutant mice is comparable with that of IGF-1-stimulated controls (Figure 6A). In addition, IGF-1 stimulation is unable to induce further Akt1 Ser473 phosphorylation (Figure 6A) suggesting that Akt1 is maximumly activated under normal physiological conditions at this time point. Quantification of the phospho-Ser473 to total Akt1 ratio confirms this observation (Figure 6C), although the decreased magnitude of the phospho:total Akt1 ratio relative to IGF-1 stimulated controls is due to the increased expression of Akt1 in *Hnrnpu* mutant mice (Figure 6D). Collectively, these observations indicate that, in the absence of *Hnrnpu*, Akt1 becomes constitutively activated and thus desensitized to IGF-1/PI3Ksignaling.

Following up on these observations, we asked whether the signaling downstream of IGF-1R was biased toward Akt1 activation. First, we examined the expression of the PI3K p110 catalytic subunit. Quantitative western blot analyses indicate that *Hnrnpu* mutant mice express ~70% more p110 than WT controls (Figures 6E and 6F). We next examined PTEN, as it is well established to oppose the Akt1 activating actions of PI3K (Laplante and Sabatini, 2012; Saxton and Sabatini, 2017). Counterintuitively, we observe the expression of PTEN to be increased >4-fold in the gastrocnemius of *Hnrnpu* mutant mice as compared with controls (Figures 6E and 6F). These observations and the accompanying reductions in body weight (Figure 2C) are consistent with a prior report indicating that increases in PTEN protein expression induce postnatal growth impairments through increases in energy expenditure (Garcia-Cao et al., 2012). Interestingly, the increases in both IGF-1R and Akt1 protein expression are positively correlated with increases in *Igf1r* (Log2FC = 0.70 ± 0.14, padj = 9.93×10^{-6}, mKO versus WT) and *Akt1* (Log2FC 0.40 ± 0.16, padj = 0.03, mKO versus WT), whereas the increase in PTEN protein is negatively correlated with *Pten* (Log2FC −0.65 ± 0.13, p = 9.67×10^{-9}, mKO versus WT) expression. Together, these observations suggest that the increase in IGF-1R and Akt1 protein expression contribute to the observed dysregulation of Akt1

activation and that post-transcriptional gene regulation of mature mRNA may also be altered in the absence of *Hnrnpu*.

Hnrnpu mKO mice share many similarities with the phenotypes of mice in which *Tsc1* (Castets et al., 2013) and *Atg7* (Masiero et al., 2009) were selectively deleted in skeletal muscle, prompting us to evaluate the downstream effects of Akt signaling on autophagy. Initiated by the essential positive regulator ULK1, and negatively regulated by Akt/mTORC1 signaling, autophagy plays crucial roles in both the maintenance of cellular metabolic homeostasis and the cellular response to stress (Rabinowitz and White, 2010). We observe a nearly 4-fold induction of ULK1 phosphorylation at Ser757 (Figures 6G and 6H) indicating an inhibition of autophagy initiation through mTORC1-dependent mechanism (Kim et al., 2011; Manning and Toker, 2017). To further corroborate this observation, we assayed for the autophagy-specific substrate and cargo receptor SQSTM1/p62, the accumulation of which is used as an indicator of autophagy impairment (Klionsky et al., 2012). Consistent with this, we observe a marked increase in the expression of SQSTM1/p62 (Figure 6G) in *Hnrnpu* mutants as compared with controls, further corroborating our observations of autophagy impairment in the absence of *Hnrnpu*. Together, these data indicate that the constitutive activation of Akt leads to an increase in mTORC1-mediated inhibition of autophagy.

The postnatal growth of skeletal muscle up to ~P21 is primarily due to the satellite cell contributions to myofiber volume and myonuclei content, after which myonuclear and satellite cell content stabilizes and hypertrophic signaling begins to dominate (White et al., 2010). As such, we sought to determine whether the satellite cell contributions to muscle growth at this time point masked PI3K/Akt signaling derangements. Quantitative western blot analyses of gastrocnemius muscles of control and mKO mice at P21 indicate no significant differences in the expression or activation of IGF-1R, PI3K p110, Akt1, and PTEN (Figure 6I), indicating the IGF-1/PI3K/Akt signaling is unaltered in *Hnrnpu* mutants at this time point. In addition, the SQSTM1/p62 protein expression in WT and *Hnrnpu* mutants at P21 (Figure 6I) is comparable with that of *Hnrnpu* mutants at 3 months of age (Figures 6G and S5). Collectively, these data indicate that *Hnrnpu* is essential for the normal physiological activation of Akt signaling and its responsiveness to IGF-1 stimulation.

DISCUSSION

The dysregulation of IGF-1/PI3K/Akt/mTOR signaling is associated with a diverse array of pathological conditions including cancer, cardiovascular disease, inflammatory and autoimmune disorders, and insulin resistance and type 2 diabetes (Manning and Toker, 2017; Saxton and Sabatini, 2017). In skeletal muscle, Akt signaling is a key regulator of glycolytic muscle homeostasis, hypertrophic growth, and metabolism through its activation of mTOR-dependent anabolic processes and simultaneous inhibition of catabolic processes. Alternative splicing plays a crucial role in muscle development, as genetic mutations in both splice sites and RNA-binding proteins involved in splicing regulation playing causal roles in the pathogenesis of neuromuscular disorders (Ho et al., 2005; Lin et al., 2006; Philips et al., 1998; Runfola et al., 2015). We demonstrate that skeletal muscle-specific deletion of *Hnrnpu* leads to an adult-onset myopathy with selective muscle wasting, fibrosis, and broad changes in both the expression and splicing of genes. In addition, dysregulated splicing is increasingly recognized as a causal factor promoting cellular dysfunction through changes in the binding properties, enzymatic activities, and intracellular localization of a large percentage of the proteome (Tress et al., 2007). Accordingly, our data in the muscles of *Hnrnpu* mutants demonstrate the constitutive activation of Akt signaling and its desensitization to IGF-1 stimulation. Of the individual muscles analyzed, the soleus was the only muscle without changes in myofiber cross-sectional area. This is in contrast with the non-significant trend and the significantly marked reduction in myofiber cross-sectional areas observed in the tibialis anterior and gastrocnemius, respectively. Although the cellular adaptations underlying the distinct growth responses to *Hnrnpu* deletion in each of these muscles are unclear, differences in functional utilization (e.g., ankle extensor versus ankle flexor) as well as metabolic adaptations specific to each individual muscle likely contribute.

In mice, both the autophosphorylation of IGF-1R and the sensitivity of Akt1 to IGF-1 are decreased with age (Akasaki et al., 2014). Our results in young *Hnrnpu* mutants indicate that the autophosphorylation of IGF-1R in response to IGF-1 is unaltered, whereas the phospho-activation of Akt1 is desensitized to IGF-1. These observations indicate that hnRNP-U is essential for the normal signaling activities downstream of IGF-1R and suggest an hnRNP-U-independent mechanism modulates the age-associated changes in IGF-1R activation. In contrast with 1-year-old non-sarcopenic WT mice (Akasaki et al., 2014), we observe Akt1 to be

constitutively active under normal physiological conditions in the atrophied muscles of *Hnrnpu* mutants, suggesting that other processes, in addition to Akt activation, are required for the hypertrophic growth of muscle. Short-term activation of Akt1 signaling induces changes in the expression of genes critical for the activity of pathways involved in the production and storage of energy and nutrients (Wu et al., 2017) in parallel with hypertrophic growth (Izumiya et al., 2008b; Wu et al., 2017). Autophagy is an essential process for the maintenance of cellular homeostasis that may be further induced in response to cellular stress to reduce organelles and macromolecules into amino acids, nucleosides, fatty acids, and sugars in support of cellular growth and survival (Rabinowitz and White, 2010). Although it is impaired by Akt/mTOR hypertrophic signaling (Manning and Toker, 2017), insufficient and excessive autophagy negatively impacts muscle (Mammucari et al., 2007; Masiero et al., 2009), suggesting an inflection point between an autophagic flux that supports muscle hypertrophy and that which promotes muscle wasting. The constitutive activation of Akt in *Hnrnpu* mutants coincides with both impaired autophagy and an increase in ULK1 inhibitory phosphorylation at S757 and is consistent with prior reports indicating that increased mTORC1 activity is responsible for the observed impairments in autophagy (Castets et al., 2013; Kim et al., 2011).

Muscle energy production may be divided into anaerobic metabolism, which provides energy from glycolysis for rapid movements, and mitochondrial regulated aerobic metabolism for sustained exercise (Zierath and Hawley, 2004). The sensing of nutrient availability and the transport of extracellular nutrients into the cell are tightly regulated by a meshwork of interconnected signaling pathways that include Akt and mTORC1 (Broer and Broer, 2017; Efeyan et al., 2015). Dysregulation of energy metabolism and nutrient insufficiencies are associated with the muscle atrophy and dysfunction known to occur with advancing age, cachexia, and multiple myopathies (Cohen et al., 2015; Koopman et al., 2014; Marcell, 2003; Petruzzelli and Wagner, 2016). The transcriptional profile of *Hnrnpu* mutants indicates that genes involved in metabolic processes, including energy production, nutrient sensing and transport, and signal transduction are both repressed and mis-spliced, suggesting that their biochemical activities and/or intracellular localization is altered. The observations of constitutively active Akt, and a marked increase in PTEN expression, would suggest an increase in the demand for amino acids necessary to support hypertrophic growth (Wu et al., 2017), as well as an increase in energy expenditures (Garcia-Cao et al., 2012). The significant increases in *Asns*, *Fgf21*, and *Gdf15* expression are consistent with a state of nutritional and metabolic stress (Broer and Broer, 2017; Fisher and Maratos-Flier, 2016; Patel et al., 2019) and are in agreement with prior analyses of gastrocnemius muscle expressing a constitutively active form of Akt (Wu et al., 2017). In addition, the marked increase in *Sln* would suggest an increase in mitochondrial biogenesis and oxidative metabolism (Maurya et al., 2018), whereas the increases in *Mthfd2* and *Psat1* are consistent with compensatory mechanisms to mitigate mitochondrial and oxidative stress (Nilsson et al., 2014; Tyynismaa et al., 2010; Yang and Vousden, 2016).

Tissue-specific and ubiquitously expressed RNA-binding proteins cooperatively interact with the regulatory elements both within a nascent transcript and of the spliceosome for context-dependent tissue-specific mRNA splicing (Fu and Ares, 2014; Wang et al., 2008). Prior reports have demonstrated the importance of skeletal muscle enriched splicing factors Rbfox1/2 (Singh et al., 2018), RBM20 (Guo et al., 2012), and RBM24 (Yang et al., 2014) in the development, functionality, and growth of muscle. Skeletal muscle accounts for approximately 50% of the nearly 50-fold increase in body weight during murine post-natal development (Allen et al., 1979). During this time, a large percentage of the transcriptome undergoes extensive temporal-dependent changes in alternative splicing that occur largely independent of changes in gene expression (Brinegar et al., 2017), suggesting that the temporal changes in protein isoform expression are critical for the post-natal physiological growth of skeletal muscle. In addition, the increasing number of whole transcriptome analyses of physiologically normal, endurance trained, hypertrophic, and atrophying skeletal muscle (Ehmsen et al., 2019; Lindholm et al., 2016; Llano-Diez et al., 2019; Shavlakadze et al., 2019; Wu et al., 2017) provides unique molecular insights into its growth and adaptive responses. Our whole transcriptome analyses describe the changes in gene expression and splicing associated with the myopathy phenotype of *Hnrnpu* mutants, identifying considerable enrichment for the mis-expression/splicing of genes associated with signal transduction, metabolic processes, and inflammation. Although it may be tempting to draw conclusions based upon these observations given the seemingly ubiquitous enrichment for metabolic and inflammatory genes among these datasets, care must be taken with such interpretations given the differences in experimental models and the uncertainty of whether such transcriptome changes are the primary effect, or a compensatory effect due to changes in muscle physiology. In addition, hnRNP-U is known to enhance the transcript stability of a few select genes (Yugami et al., 2007), which may suggest

that gene expression, as influenced by mRNA stability, may be similarly influenced by exon inclusion/exclusion. Although the relationship between mRNA stability and splicing is not well understood and likely regulated on a gene- and intron/exon-specific basis (Clement et al., 1999; Nott et al., 2003), the possibility that this may contribute to our observations is intriguing.

Collectively, our studies link *Hnrnpu* to the proper expression and splicing of genes underlying the physiological growth of skeletal muscle. Our data would suggest that the muscles of *Hnrnpu* mutants are under cellular and metabolic stress due to dysregulation of the cellular feedback mechanisms limiting Akt/mTOR signaling in response to energy and/or nutrient insufficiency. Future detailed analyses dissecting the impact of alternative splicing dysregulation on the feedback mechanism limiting Akt/mTOR may provide novel insights to the pathogenesis of muscle wasting disorders.

Limitations of the Study

We demonstrate that loss of *Hnrnpu* in skeletal muscle causes impaired post-natal hypertrophic growth and changes in the expression and splicing of numerous genes involved in signal transduction and metabolic processes. Our data strongly suggest that impaired muscle growth due to the loss of hnRNP-U is biased toward muscles with a greater content of fast glycolytic, rather than slow oxidative, myofibers but cannot definitively confirm this observation at the level of the individual myofiber subtype. Given the temporal lag between *in vivo* Cre activation and the time point at which whole transcriptome analyses were performed, we are unable to discern between the primary and secondary effects on the transcriptome, and its impact on muscle physiology, owing to the loss of hnRNP-U. RNA-binding proteins play crucial roles in modulating the stability, structure, and splicing of transcripts (Hentze et al., 2018), making it difficult to discern between these functions as these processes are interrelated. In cell culture model systems, hnRNPU is known to bind a purine-rich consensus sequence (KGRGKRV) to modulate both the splicing of nascent transcripts (Huelga et al., 2012; Xiao et al., 2012) and the stability of mRNA (Yugami et al., 2007). Whether skeletal muscle hnRNP-U binds a similar set of nascent transcripts and enhances mRNA stability is unknown and warrants future investigations. Although our transcriptional data and signaling analyses are consistent with prior reports of cellular and metabolic stress in muscle (Izumiya et al., 2008a; Khan et al., 2017; Suomalainen et al., 2011; Tyynismaa et al., 2010), metabolic profiling and detailed molecular analyses of splice variant functional analyses will be needed to better understand the mechanistic linkages between splice variant expression and the regulation of Akt/mTOR signaling in muscle physiology.

Resource Availability

Lead Contact

Ronald L Neppl (rneppl@bwh.harvard.edu).

Materials Availability

Further information and requests for ressources and reagents should be directed to and will be fullfilled by the Lead Contact.

Data and Code Availability

The accession number for the RNA sequencing data reported in this paper is NCBI Gene Expression Omnibus: GSE145712. No new computational tools were developed in this project. The code for usage of existing tools as described is available upon request.

METHODS

All methods can be found in the accompanying Transparent Methods supplemental file.

SUPPLEMENTAL INFORMATION

Supplemental Information can be found online at https://doi.org/10.1016/j.isci.2020.101319.

ACKNOWLEDGMENTS

The authors would like to thank Dr. Tom Maniatis for the Hnrnpu mouse line and Teri Bowman for her technical assistance with histology processing. This work was supported by the National Institutes of Health K76AG059996 to I.S., a Research Education Component Grant from the National Institutes of Health

National Institute on Aging (P30AG031679) funded Boston Claude D. Pepper Older Americans Independence Center to R.L.N., and funds from the Brigham and Women's Hospital Department of Orthopaedic Surgery to R.L.N.

AUTHOR CONTRIBUTIONS

D.B., B.D.M., K.B., B.L., E.-J.L., and Y.Z. conducted experiments. D.B., B.D.M., K.B., B.L., E.-J.L., Y.Z., L.K.C., and S.e.R. analyzed data. D.B., B.D.M., K.B., and Y.Z. contributed to writing of the original draft. R.L.N. conceptualized and designed the study. R.L.N. and I.S. performed project administration, supervision, funding acquisition, and review & editing of the manuscript.

DECLARATION OF INTERESTS

The authors declare no competing interests.

Received: February 20, 2020
Revised: April 30, 2020
Accepted: June 24, 2020
Published: July 24, 2020

REFERENCES

Akasaki, Y., Ouchi, N., Izumiya, Y., Bernardo, B.L., Lebrasseur, N.K., and Walsh, K. (2014). Glycolytic fast-twitch muscle fiber restoration counters adverse age-related changes in body composition and metabolism. Aging Cell *13*, 80–91.

Allen, R.E., Merkel, R.A., and Young, R.B. (1979). Cellular aspects of muscle growth: myogenic cell proliferation. J. Anim. Sci. *49*, 115–127.

Balasubramanian, M.N., Butterworth, E.A., and Kilberg, M.S. (2013). Asparagine synthetase: regulation by cell stress and involvement in tumor biology. Am. J. Physiol. Endocrinol. Metab. *304*, E789–E799.

Baumann, C.A., Ribon, V., Kanzaki, M., Thurmond, D.C., Mora, S., Shigematsu, S., Bickel, P.E., Pessin, J.E., and Saltiel, A.R. (2000). CAP defines a second signalling pathway required for insulin-stimulated glucose transport. Nature *407*, 202–207.

Biamonti, G., and Caceres, J.F. (2009). Cellular stress and RNA splicing. Trends Biochem. Sci. *34*, 146–153.

Bodine, S.C., Latres, E., Baumhueter, S., Lai, V.K., Nunez, L., Clarke, B.A., Poueymirou, W.T., Panaro, F.J., Na, E., Dharmarajan, K., et al. (2001). Identification of ubiquitin ligases required for skeletal muscle atrophy. Science *294*, 1704–1708.

Brinegar, A.E., Xia, Z., Loehr, J.A., Li, W., Rodney, G.G., and Cooper, T.A. (2017). Extensive alternative splicing transitions during postnatal skeletal muscle development are required for calcium handling functions. Elife *6*, e27192.

Broer, S., and Broer, A. (2017). Amino acid homeostasis and signalling in mammalian cells and organisms. Biochem. J. *474*, 1935–1963.

Cai, R., Yu, T., Huang, C., Xia, X., Liu, X., Gu, J., Xue, S., Yeh, E.T., and Cheng, J. (2012). SUMO-specific protease 1 regulates mitochondrial biogenesis through PGC-1alpha. J. Biol. Chem. *287*, 44464–44470.

Castets, P., Lin, S., Rion, N., Di Fulvio, S., Romanino, K., Guridi, M., Frank, S., Tintignac, L.A., Sinnreich, M., and Ruegg, M.A. (2013). Sustained activation of mTORC1 in skeletal muscle inhibits constitutive and starvation-induced autophagy and causes a severe, late-onset myopathy. Cell Metab. *17*, 731–744.

Chung, H.K., Ryu, D., Kim, K.S., Chang, J.Y., Kim, Y.K., Yi, H.S., Kang, S.G., Choi, M.J., Lee, S.E., Jung, S.B., et al. (2017). Growth differentiation factor 15 is a myomitokine governing systemic energy homeostasis. J. Cell Biol. *216*, 149–165.

Clement, J.Q., Qian, L., Kaplinsky, N., and Wilkinson, M.F. (1999). The stability and fate of a spliced intron from vertebrate cells. RNA *5*, 206–220.

Cohen, S., Nathan, J.A., and Goldberg, A.L. (2015). Muscle wasting in disease: molecular mechanisms and promising therapies. Nat. Rev. Drug Discov. *14*, 58–74.

Demontis, F., Piccirillo, R., Goldberg, A.L., and Perrimon, N. (2013). Mechanisms of skeletal muscle aging: insights from Drosophila and mammalian models. Dis. Model. Mech. *6*, 1339–1352.

Dutertre, M., Sanchez, G., Barbier, J., Corcos, L., and Auboeuf, D. (2011). The emerging role of pre-messenger RNA splicing in stress responses: sending alternative messages and silent messengers. RNA Biol. *8*, 740–747.

Efeyan, A., Comb, W.C., and Sabatini, D.M. (2015). Nutrient-sensing mechanisms and pathways. Nature *517*, 302–310.

Ehmsen, J.T., Kawaguchi, R., Mi, R., Coppola, G., and Hoke, A. (2019). Longitudinal RNA-Seq analysis of acute and chronic neurogenic skeletal muscle atrophy. Sci. Data *6*, 179.

Emery, A.E. (2002). The muscular dystrophies. Lancet *359*, 687–695.

Eom, G.H., Kim, K.B., Kim, J.H., Kim, J.Y., Kim, J.R., Kee, H.J., Kim, D.W., Choe, N., Park, H.J., Son, H.J., et al. (2011). Histone methyltransferase SETD3 regulates muscle differentiation. J. Biol. Chem. *286*, 34733–34742.

Ernste, F.C., and Reed, A.M. (2013). Idiopathic inflammatory myopathies: current trends in pathogenesis, clinical features, and up-to-date treatment recommendations. Mayo Clin. Proc. *88*, 83–105.

Faustino, N.A., and Cooper, T.A. (2003). Pre-mRNA splicing and human disease. Genes Dev. *17*, 419–437.

Fisher, F.M., and Maratos-Flier, E. (2016). Understanding the physiology of FGF21. Annu. Rev. Physiol. *78*, 223–241.

Fu, X.D., and Ares, M., Jr. (2014). Context-dependent control of alternative splicing by RNA-binding proteins. Nat. Rev. Genet. *15*, 689–701.

Garcia-Cao, I., Song, M.S., Hobbs, R.M., Laurent, G., Giorgi, C., de Boer, V.C., Anastasiou, D., Ito, K., Sasaki, A.T., Rameh, L., et al. (2012). Systemic elevation of PTEN induces a tumor-suppressive metabolic state. Cell *149*, 49–62.

Geuens, T., Bouhy, D., and Timmerman, V. (2016). The hnRNP family: insights into their role in health and disease. Hum. Genet. *135*, 851–867.

Glass, D.J. (2005). Skeletal muscle hypertrophy and atrophy signaling pathways. Int. J. Biochem. Cell Biol. *37*, 1974–1984.

Guo, W., Schafer, S., Greaser, M.L., Radke, M.H., Liss, M., Govindarajan, T., Maatz, H., Schulz, H., Li, S., Parrish, A.M., et al. (2012). RBM20, a gene for hereditary cardiomyopathy, regulates titin splicing. Nat. Med. *18*, 766–773.

Hentze, M.W., Castello, A., Schwarzl, T., and Preiss, T. (2018). A brave new world of RNA-binding proteins. Nat. Rev. Mol. Cell Biol. *19*, 327–341.

Ho, T.H., Bundman, D., Armstrong, D.L., and Cooper, T.A. (2005). Transgenic mice expressing CUG-BP1 reproduce splicing mis-regulation

observed in myotonic dystrophy. Hum. Mol. Genet. *14*, 1539–1547.

Huelga, S.C., Vu, A.Q., Arnold, J.D., Liang, T.Y., Liu, P.P., Yan, B.Y., Donohue, J.P., Shiue, L., Hoon, S., Brenner, S., et al. (2012). Integrative genome-wide analysis reveals cooperative regulation of alternative splicing by hnRNP proteins. Cell Rep. *1*, 167–178.

Ivetac, I., Gurung, R., Hakim, S., Horan, K.A., Sheffield, D.A., Binge, L.C., Majerus, P.W., Tiganis, T., and Mitchell, C.A. (2009). Regulation of PI(3)K/Akt signalling and cellular transformation by inositol polyphosphate 4-phosphatase-1. EMBO Rep. *10*, 487–493.

Izumiya, Y., Bina, H.A., Ouchi, N., Akasaki, Y., Kharitonenkov, A., and Walsh, K. (2008a). FGF21 is an Akt-regulated myokine. FEBS Lett. *582*, 3805–3810.

Izumiya, Y., Hopkins, T., Morris, C., Sato, K., Zeng, L., Viereck, J., Hamilton, J.A., Ouchi, N., LeBrasseur, N.K., and Walsh, K. (2008b). Fast/Glycolytic muscle fiber growth reduces fat mass and improves metabolic parameters in obese mice. Cell Metab. *7*, 159–172.

Khan, N.A., Nikkanen, J., Yatsuga, S., Jackson, C., Wang, L., Pradhan, S., Kivela, R., Pessia, A., Velagapudi, V., and Suomalainen, A. (2017). mTORC1 regulates mitochondrial integrated stress response and mitochondrial myopathy progression. Cell Metab. *26*, 419–428 e415.

Kim, J., Kundu, M., Viollet, B., and Guan, K.L. (2011). AMPK and mTOR regulate autophagy through direct phosphorylation of Ulk1. Nat. Cell Biol. *13*, 132–141.

Klionsky, D.J., Abdalla, F.C., Abeliovich, H., Abraham, R.T., Acevedo-Arozena, A., Adeli, K., Agholme, L., Agnello, M., Agostinis, P., Aguirre-Ghiso, J.A., et al. (2012). Guidelines for the use and interpretation of assays for monitoring autophagy. Autophagy *8*, 445–544.

Koopman, R., Ly, C.H., and Ryall, J.G. (2014). A metabolic link to skeletal muscle wasting and regeneration. Front. Physiol. *5*, 32.

Lai, K.M., Gonzalez, M., Poueymirou, W.T., Kline, W.O., Na, E., Zlotchenko, E., Stitt, T.N., Economides, A.N., Yancopoulos, G.D., and Glass, D.J. (2004). Conditional activation of akt in adult skeletal muscle induces rapid hypertrophy. Mol. Cell. Biol. *24*, 9295–9304.

Laplante, M., and Sabatini, D.M. (2012). mTOR signaling in growth control and disease. Cell *149*, 274–293.

Lee, Y., and Rio, D.C. (2015). Mechanisms and regulation of alternative pre-mRNA splicing. Annu. Rev. Biochem. *84*, 291–323.

Li, M., Zhuang, Y., Batra, R., Thomas, J.D., Li, M., Nutter, C.A., Scotti, M.M., Carter, H.A., Wang, Z.J., Huang, X.S., et al. (2020). HNRNPA1-induced spliceopathy in a transgenic mouse model of myotonic dystrophy. Proc. Natl. Acad. Sci. U S A *117*, 5472–5477.

Lin, L., Yee, S.W., Kim, R.B., and Giacomini, K.M. (2015). SLC transporters as therapeutic targets: emerging opportunities. Nat. Rev. Drug Discov. *14*, 543–560.

Lin, X., Miller, J.W., Mankodi, A., Kanadia, R.N., Yuan, Y., Moxley, R.T., Swanson, M.S., and Thornton, C.A. (2006). Failure of MBNL1-dependent post-natal splicing transitions in myotonic dystrophy. Hum. Mol. Genet. *15*, 2087–2097.

Lindholm, M.E., Giacomello, S., Werne Solnestam, B., Fischer, H., Huss, M., Kjellqvist, S., and Sundberg, C.J. (2016). The impact of endurance training on human skeletal muscle memory, global isoform expression and novel transcripts. PLoS Genet. *12*, e1006294.

Llano-Diez, M., Fury, W., Okamoto, H., Bai, Y., Gromada, J., and Larsson, L. (2019). RNA-sequencing reveals altered skeletal muscle contraction, E3 ligases, autophagy, apoptosis, and chaperone expression in patients with critical illness myopathy. Skelet. Muscle *9*, 9.

Mammucari, C., Milan, G., Romanello, V., Masiero, E., Rudolf, R., Del Piccolo, P., Burden, S.J., Di Lisi, R., Sandri, C., Zhao, J., et al. (2007). FoxO3 controls autophagy in skeletal muscle in vivo. Cell Metab. *6*, 458–471.

Manning, B.D., and Toker, A. (2017). AKT/PKB signaling: navigating the network. Cell *169*, 381–405.

Marcell, T.J. (2003). Sarcopenia: causes, consequences, and preventions. J. Gerontol. A. Biol. Sci. Med. Sci. *58*, M911–M916.

Martinez-Contreras, R., Cloutier, P., Shkreta, L., Fisette, J.F., Revil, T., and Chabot, B. (2007). hnRNP proteins and splicing control. Adv. Exp. Med. Biol. *623*, 123–147.

Masiero, E., Agatea, L., Mammucari, C., Blaauw, B., Loro, E., Komatsu, M., Metzger, D., Reggiani, C., Schiaffino, S., and Sandri, M. (2009). Autophagy is required to maintain muscle mass. Cell Metab. *10*, 507–515.

Maurya, S.K., Herrera, J.L., Sahoo, S.K., Reis, F.C.G., Vega, R.B., Kelly, D.P., and Periasamy, M. (2018). Sarcolipin signaling promotes mitochondrial biogenesis and oxidative metabolism in skeletal muscle. Cell Rep. *24*, 2919–2931.

Merkin, J., Russell, C., Chen, P., and Burge, C.B. (2012). Evolutionary dynamics of gene and isoform regulation in Mammalian tissues. Science *338*, 1593–1599.

Miniou, P., Tiziano, D., Frugier, T., Roblot, N., Le Meur, M., and Melki, J. (1999). Gene targeting restricted to mouse striated muscle lineage. Nucleic Acids Res. *27*, e27.

Nilsson, R., Jain, M., Madhusudhan, N., Sheppard, N.G., Strittmatter, L., Kampf, C., Huang, J., Asplund, A., and Mootha, V.K. (2014). Metabolic enzyme expression highlights a key role for MTHFD2 and the mitochondrial folate pathway in cancer. Nat. Commun. *5*, 3128.

Nott, A., Meislin, S.H., and Moore, M.J. (2003). A quantitative analysis of intron effects on mammalian gene expression. RNA *9*, 607–617.

Nowak, M., Suenkel, B., Porras, P., Migotti, R., Schmidt, F., Kny, M., Zhu, X., Wanker, E.E., Dittmar, G., Fielitz, J., et al. (2019). DCAF8, a novel MuRF1 interaction partner, promotes muscle atrophy. J. Cell Sci. *132*, jcs233395.

Otera, H., Wang, C., Cleland, M.M., Setoguchi, K., Yokota, S., Youle, R.J., and Mihara, K. (2010). Mff is an essential factor for mitochondrial recruitment of Drp1 during mitochondrial fission in mammalian cells. J. Cell Biol. *191*, 1141–1158.

Pan, Q., Shai, O., Lee, L.J., Frey, B.J., and Blencowe, B.J. (2008). Deep surveying of alternative splicing complexity in the human transcriptome by high-throughput sequencing. Nat. Genet. *40*, 1413–1415.

Patel, S., Alvarez-Guaita, A., Melvin, A., Rimmington, D., Dattilo, A., Miedzybrodzka, E.L., Cimino, I., Maurin, A.C., Roberts, G.P., Meek, C.L., et al. (2019). GDF15 provides an endocrine signal of nutritional stress in mice and humans. Cell Metab. *29*, 707–718.e8.

Petruzzelli, M., and Wagner, E.F. (2016). Mechanisms of metabolic dysfunction in cancer-associated cachexia. Genes Dev. *30*, 489–501.

Philips, A.V., Timchenko, L.T., and Cooper, T.A. (1998). Disruption of splicing regulated by a CUG-binding protein in myotonic dystrophy. Science *280*, 737–741.

Rabinowitz, J.D., and White, E. (2010). Autophagy and metabolism. Science *330*, 1344–1348.

Risson, V., Mazelin, L., Roceri, M., Sanchez, H., Moncollin, V., Corneloup, C., Richard-Bulteau, H., Vignaud, A., Baas, D., Defour, A., et al. (2009). Muscle inactivation of mTOR causes metabolic and dystrophin defects leading to severe myopathy. J. Cell Biol. *187*, 859–874.

Rovira Gonzalez, Y.I., Moyer, A.L., LeTexier, N.J., Bratti, A.D., Feng, S., Sun, C., Liu, T., Mula, J., Jha, P., Iyer, S.R., et al. (2019). Mss51 deletion enhances muscle metabolism and glucose homeostasis in mice. JCI Insight *4*, e122247.

Runfola, V., Sebastian, S., Dilworth, F.J., and Gabellini, D. (2015). Rbfox proteins regulate tissue-specific alternative splicing of Mef2D required for muscle differentiation. J. Cell Sci. *128*, 631–637.

Sartori, R., Schirwis, E., Blaauw, B., Bortolanza, S., Zhao, J., Enzo, E., Stantzou, A., Mouisel, E., Toniolo, L., Ferry, A., et al. (2013). BMP signaling controls muscle mass. Nat. Genet. *45*, 1309–1318.

Saxton, R.A., and Sabatini, D.M. (2017). mTOR signaling in growth, metabolism, and disease. Cell *168*, 960–976.

Scotti, M.M., and Swanson, M.S. (2016). RNA mis-splicing in disease. Nat. Rev. Genet. *17*, 19–32.

Seaborne, R.A., Strauss, J., Cocks, M., Shepherd, S., O'Brien, T.D., van Someren, K.A., Bell, P.G., Murgatroyd, C., Morton, J.P., Stewart, C.E., et al. (2018). Human skeletal muscle possesses an epigenetic memory of hypertrophy. Sci. Rep. *8*, 1898.

Shavlakadze, T., Morris, M., Fang, J., Wang, S.X., Zhu, J., Zhou, W., Tse, H.W., Mondragon-Gonzalez, R., Roma, G., and Glass, D.J. (2019). Age-related gene expression signature in rats demonstrate early, late, and linear transcriptional changes from multiple tissues. Cell Rep *28*, 3263–3273.e3.

Shen, S., Park, J.W., Lu, Z.X., Lin, L., Henry, M.D., Wu, Y.N., Zhou, Q., and Xing, Y. (2014). rMATS:

robust and flexible detection of differential alternative splicing from replicate RNA-Seq data. Proc. Natl. Acad. Sci. U S A *111*, E5593–E5601.

Singh, R.K., Kolonin, A.M., Fiorotto, M.L., and Cooper, T.A. (2018). Rbfox-splicing factors maintain skeletal muscle mass by regulating Calpain3 and proteostasis. Cell Rep. *24*, 197–208.

Suomalainen, A., Elo, J.M., Pietilainen, K.H., Hakonen, A.H., Sevastianova, K., Korpela, M., Isohanni, P., Marjavaara, S.K., Tyni, T., Kiuru-Enari, S., et al. (2011). FGF-21 as a biomarker for muscle-manifesting mitochondrial respiratory chain deficiencies: a diagnostic study. Lancet Neurol. *10*, 806–818.

Tress, M.L., Martelli, P.L., Frankish, A., Reeves, G.A., Wesselink, J.J., Yeats, C., Olason, P.I., Albrecht, M., Hegyi, H., Giorgetti, A., et al. (2007). The implications of alternative splicing in the ENCODE protein complement. Proc. Natl. Acad. Sci. U S A *104*, 5495–5500.

Tyynismaa, H., Carroll, C.J., Raimundo, N., Ahola-Erkkila, S., Wenz, T., Ruhanen, H., Guse, K., Hemminki, A., Peltola-Mjosund, K.E., Tulkki, V., et al. (2010). Mitochondrial myopathy induces a starvation-like response. Hum. Mol. Genet. *19*, 3948–3958.

Vance, C., Rogelj, B., Hortobagyi, T., De Vos, K.J., Nishimura, A.L., Sreedharan, J., Hu, X., Smith, B., Ruddy, D., Wright, P., et al. (2009). Mutations in FUS, an RNA processing protein, cause familial amyotrophic lateral sclerosis type 6. Science *323*, 1208–1211.

Wang, E.T., Sandberg, R., Luo, S., Khrebtukova, I., Zhang, L., Mayr, C., Kingsmore, S.F., Schroth, G.P., and Burge, C.B. (2008). Alternative isoform regulation in human tissue transcriptomes. Nature *456*, 470–476.

White, R.B., Bierinx, A.S., Gnocchi, V.F., and Zammit, P.S. (2010). Dynamics of muscle fibre growth during postnatal mouse development. BMC Dev. Biol. *10*, 21.

Wu, C.L., Satomi, Y., and Walsh, K. (2017). RNA-seq and metabolomic analyses of Akt1-mediated muscle growth reveals regulation of regenerative pathways and changes in the muscle secretome. BMC Genomics *18*, 181.

Xiao, R., Tang, P., Yang, B., Huang, J., Zhou, Y., Shao, C., Li, H., Sun, H., Zhang, Y., and Fu, X.D. (2012). Nuclear matrix factor hnRNP U/SAF-A exerts a global control of alternative splicing by regulating U2 snRNP maturation. Mol. Cell *45*, 656–668.

Yang, J., Hung, L.H., Licht, T., Kostin, S., Looso, M., Khrameeva, E., Bindereif, A., Schneider, A., and Braun, T. (2014). RBM24 is a major regulator of muscle-specific alternative splicing. Dev. Cell *31*, 87–99.

Yang, M., and Vousden, K.H. (2016). Serine and one-carbon metabolism in cancer. Nat. Rev. Cancer *16*, 650–662.

Yates, T.M., Vasudevan, P.C., Chandler, K.E., Donnelly, D.E., Stark, Z., Sadedin, S., Willoughby, J., Broad Center for Mendelian, G., study, D.D.D., and Balasubramanian, M. (2017). De novo mutations in HNRNPU result in a neurodevelopmental syndrome. Am. J. Med. Genet. A *173*, 3003–3012.

Ye, J., Beetz, N., O'Keeffe, S., Tapia, J.C., Macpherson, L., Chen, W.V., Bassel-Duby, R., Olson, E.N., and Maniatis, T. (2015). hnRNP U protein is required for normal pre-mRNA splicing and postnatal heart development and function. Proc. Natl. Acad. Sci. U S A *112*, E3020–E3029.

Yen, C.L., Stone, S.J., Koliwad, S., Harris, C., and Farese, R.V., Jr. (2008). Thematic review series: glycerolipids. DGAT enzymes and triacylglycerol biosynthesis. J. Lipid Res. *49*, 2283–2301.

Yugami, M., Kabe, Y., Yamaguchi, Y., Wada, T., and Handa, H. (2007). hnRNP-U enhances the expression of specific genes by stabilizing mRNA. FEBS Lett. *581*, 1–7.

Zierath, J.R., and Hawley, J.A. (2004). Skeletal muscle fiber type: influence on contractile and metabolic properties. PLoS Biol. *2*, e348.

iScience, Volume *23*

Supplemental Information

Adult-Onset Myopathy with Constitutive Activation of Akt following the Loss of hnRNP-U

Debalina Bagchi, Benjamin D. Mason, Kodilichi Baldino, Bin Li, Eun-Joo Lee, Yuteng Zhang, Linh Khanh Chu, Sherif El Raheb, Indranil Sinha, and Ronald L. Neppl

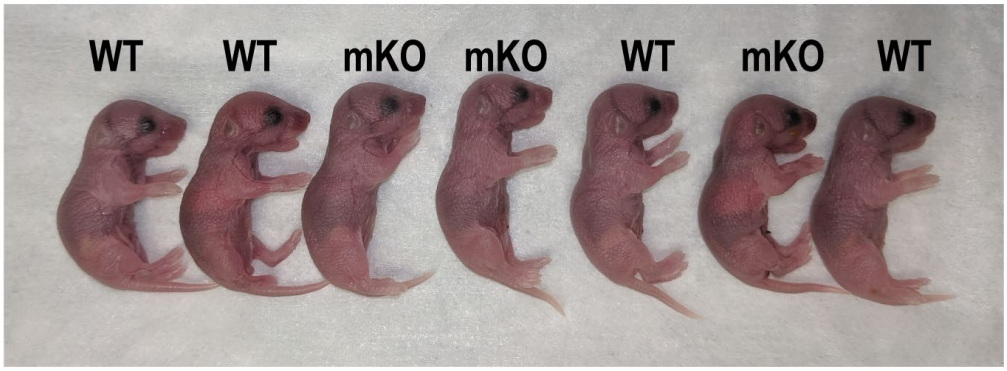

Fig. S1: Hnrnpu mKO mice are phenotypically normal at birth, Related to Figure 1. Representative image of WT and mKO littermates.

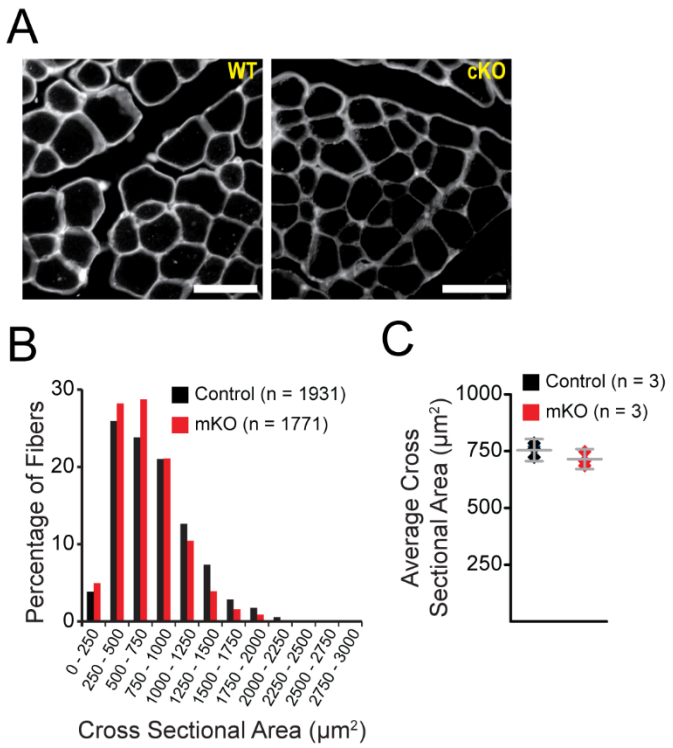

Fig. S2: Morphometric analysis of tibialis anterior muscle at P21, Related to Figure 1. (A) Laminin stained cross sections. (B) Histogram of myofiber size distribution. (C) Average myofiber cross sectional area for each biological replicate. Data are mean ± standard deviation from n = 3 mice per group. The scale bar is 50 microns.

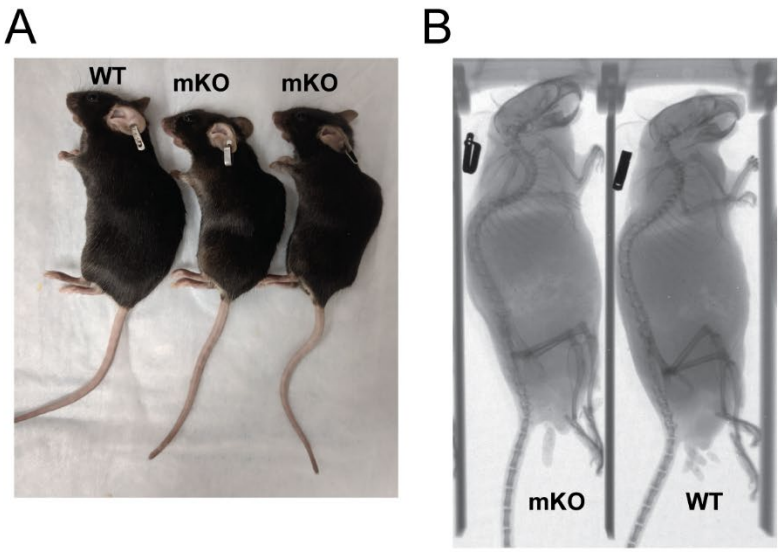

Fig. S3: Hnrnpu mKO develop kyphosis, Related to Figure 2. (A) Representative images of female littermates at 5 months of age. (B) Representative X-ray micrograph of male littermates at 7 months of age.

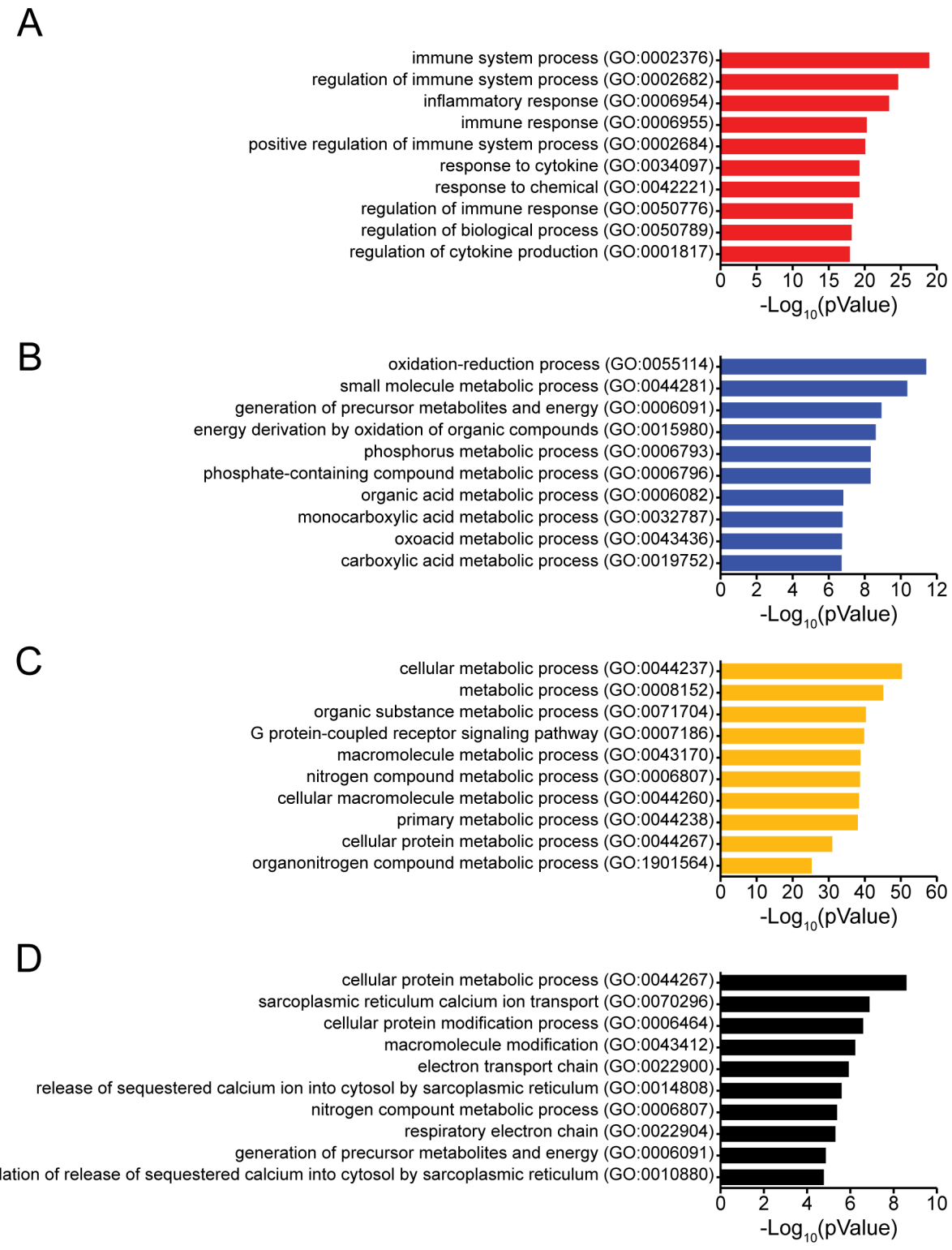

Fig. S4: Gene Ontology Enrichment Analyses of RNAseq data, Related to Figure 5. Top GO terms of genes whose expression is increased (A), decreased (B), differentially spliced (C), and both differentially spliced and decreased (D) in expression in Hnrnpu mutants with respect to control.

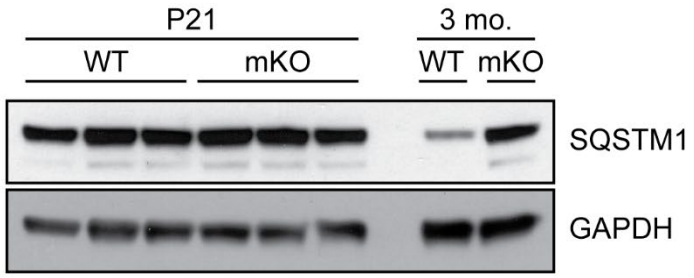

Fig. S5: Hnrnpu mKO mice develop autophagy impairments by 3 months of age, Related to Figure 6. Representative Western blot of SQSTM1 expression in gastrocnemius of Hnrnpu mKO and litter mate controls at P21 and 3 months of age.

Transparent Methods:

Mouse models – Generation of the Hnrnpu floxed allele has been described previously (Ye et al., 2015). Skeletal muscle specific deletion of Hnrnpu was achieved by crossing with the HSA-Cre (Miniou et al., 1999) mouse line, which expresses the Cre recombinase under the control of the human skeletal alpha-actin promoter. Hnrnpu$^{fl/fl}$ and Hnrnpu$^{fl/fl}$;HSA-Cre mice are on a mixed C57BL/6-129S background. Young (2-3 months of age) and old (24-26 months of age) C57BL/6 mice were obtained from the National Institute of Aging. All animal procedures were approved by the Institutional Animal Care and Use Committee at Brigham and Women's Hospital.

Cryoinjury model and histological analysis – Cryoinjury model was performed as previously described (Sinha et al., 2017). Briefly, mice were anesthetized with isoflurane and the skin over the tibialis anterior (TA) was depilated and prepped with sterile alcohol. An incision was made to expose the TA, at which point dry ice was applied directly to the muscle for 5 seconds. The incision was sutured closed immediately after injury. Animals were euthanized at 7 – 10 post injury for histological analyses. Ten (10) images spanning the region of regeneration were acquired per sample. The area of 10 myofibers with central nuclei were chosen randomly for measurement using ImageJ; a total of 100 myofibers were quantified per biological sample. Images were minimally manipulated in Photoshop to linearly increase contrast equally across all pixels.

IGF-1 response – In vivo signaling downstream of IGF-1 was assessed as previously described (Akasaki et al., 2014). Briefly, mice were anesthetized with isoflurane, and the skin over the gastrocnemius was depilated and prepped with sterile alcohol. Mice were injected with either recombinant human IGF-1 (100 µg), or vehicle (sterile water), directly into the gastrocnemius of the right leg using an insulin syringe. Mice were euthanized 1-hour post injection, and the gastrocnemius was excised and snap-frozen. IGF-1 was purchased from Peprotech Inc (Rocky Hill, NJ).

Immunohistochemistry and histological analyses – Hind limb muscles were excised, fixed in 4% PFA, and either cryoprotected with 30% sucrose and embedded in Tissue-Tek or dehydrated in ethanol and paraffin embedded. Transverse sections were subjected to immunostaining, nuclei counterstain, imaging, and post-processing as previously described (Neppl et al., 2017). Briefly, fixed tissues were permeabilized with 0.05% Triton X-100 for 20 minutes and blocked with 5% normal donkey serum. Primary antibodies were visualized with cyanine Cy3 or Alexa-Flour 594 conjugated antibodies (Jackson ImmunoResearch Laboratories). Images were acquired at room temperature with a Leica DMi8 microscope with either a 10x or 20x PlanFluotar objective. Approximately 10 – 15 images were acquired from each immunofluorescent stained section. Images were minimally manipulated in Photoshop to linearly increase contrast equally across all pixels.

Western Blot Analysis – Quantitative western blotting was performed, with minor modifications, according to previously described methods (Neppl et al., 2014). Briefly, tissues were homogenized in 20mM Tris HCl pH 7.5, 150mM NaCl, 1% Triton-X, Halt Protease and Phosphatase Inhibitor Cocktails (Thermo Scientific). Lysates were cleared by centrifugation at 10,000 × g for 10 minutes at 4ºC. Protein content was quantified by the DC protein assay (Bio-Rad) with known concentrations of BSA as standards. Protein concentrations were equalized by addition of an appropriate volume of lysis buffer. Primary antibodies were detected by goat anti-mouse or goat anti-rabbit HRP-conjugated secondary antibodies, and visualized with SuperSignal West Pico PLUS Chemiluminescent Substrate (ThermoFisher Scientific). Films were scanned, and protein band intensities were quantified using ImageJ.

X-Ray Imaging – Mice were anesthetized with isoflurane and imaged with the Bruker In-Vivo Extreme II Optical/X-ray system for imaging.

RNAseq and postprocessing for differential gene and splicing analysis – Total RNA from WT and cKO (n = 3, each) gastrocnemius muscle was isolated by TRIzol reagent. The sequencing library was prepared with NEBNext Ultra RNA Library Prep Kit from ribosome depleted RNA, and subjected to HiSeq2500 paired-end strand-specific. Sequencing was performed at a read depth of >60 million reads per biological sample. Following QC and trimming of adapters, reads were mapped using STAR aligner software (Dobin et al., 2013), and counted using featureCounts (Liao et al., 2014). Differential gene expression was quantified using DESeq2

(Love et al., 2014), and analysis of RNA splicing was performed using rMATS (Shen et al., 2014). RNAseq data are registered in the NCBI GEO with accession number GSE145712.

Antibodies – Anti-Akt1 (#2938), Anti-phospho-Akt1 Ser473 (#9271), anti-PTEN (#14642), anti-PI3 Kinase p110α (C73F8), anti-Phospho-IGF-I Receptor β (Tyr1135) (DA7A8), anti-IGF-I Receptor β Antibody #3027, anti-SQSTM1/p62 Antibody (#5114), anti-Phospho-ULK1 Ser757 (#6888) and anti-β-Tubulin (#2146) were purchased from Cell Signaling Technologies. Anti-hnRNP-U (ab20666) was purchased from Abcam and anti-Atg1/ULK1 was purchased from Sigma-Aldrich. Anti-GAPDH, clone 6C5 was purchased from EMD Millipore.

Supplemental References

Akasaki, Y., Ouchi, N., Izumiya, Y., Bernardo, B.L., Lebrasseur, N.K., and Walsh, K. (2014). Glycolytic fast-twitch muscle fiber restoration counters adverse age-related changes in body composition and metabolism. Aging Cell *13*, 80-91.

Dobin, A., Davis, C.A., Schlesinger, F., Drenkow, J., Zaleski, C., Jha, S., Batut, P., Chaisson, M., and Gingeras, T.R. (2013). STAR: ultrafast universal RNA-seq aligner. Bioinformatics *29*, 15-21.

Liao, Y., Smyth, G.K., and Shi, W. (2014). featureCounts: an efficient general purpose program for assigning sequence reads to genomic features. Bioinformatics *30*, 923-930.

Love, M.I., Huber, W., and Anders, S. (2014). Moderated estimation of fold change and dispersion for RNA-seq data with DESeq2. Genome Biol *15*, 550.

Miniou, P., Tiziano, D., Frugier, T., Roblot, N., Le Meur, M., and Melki, J. (1999). Gene targeting restricted to mouse striated muscle lineage. Nucleic Acids Res *27*, e27.

Neppl, R.L., Kataoka, M., and Wang, D.Z. (2014). Crystallin-alphaB Regulates Skeletal Muscle Homeostasis via Modulation of Argonaute2 Activity. J Biol Chem *289*, 17240-17248.

Neppl, R.L., Wu, C.L., and Walsh, K. (2017). lncRNA Chronos is an aging-induced inhibitor of muscle hypertrophy. J Cell Biol *216*, 3497-3507.

Shen, S., Park, J.W., Lu, Z.X., Lin, L., Henry, M.D., Wu, Y.N., Zhou, Q., and Xing, Y. (2014). rMATS: robust and flexible detection of differential alternative splicing from replicate RNA-Seq data. Proc Natl Acad Sci U S A *111*, E5593-5601.

Sinha, I., Sakthivel, D., Olenchock, B.A., Kruse, C.R., Williams, J., Varon, D.E., Smith, J.D., Madenci, A.L., Nuutila, K., and Wagers, A.J. (2017). Prolyl Hydroxylase Domain-2 Inhibition Improves Skeletal Muscle Regeneration in a Male Murine Model of Obesity. Front Endocrinol (Lausanne) *8*, 153.

Ye, J., Beetz, N., O'Keeffe, S., Tapia, J.C., Macpherson, L., Chen, W.V., Bassel-Duby, R., Olson, E.N., and Maniatis, T. (2015). hnRNP U protein is required for normal pre-mRNA splicing and postnatal heart development and function. Proc Natl Acad Sci U S A *112*, E3020-3029.